Reviewer 1

Interactive comment on “Simulation of SOA Formation from the Photooxidation of Monoalkylbenzenes in the Presence of Aqueous Aerosols Containing Electrolytes under Various NO_x Levels” by Chufan Zhou et al.

Chufan Zhou, Myoseon Jang, and Zechen Yu
mjang@ufl.edu

Received and published: 22 November 2018

We thank reviewer Dr. Gorkowski for the valuable comments on the manuscript.

Major comment: Dynamic α_i

I understand the mass-based stoichiometric coefficient (α_i), has to be dynamic to capture the full evolution of the aerosol mass. It is not clear on page 5 line 7, if the dynamic reconstruction is a fit to smog chamber data or not. Section 3.1 reads as if α_i was fitted at the beginning and ending conditions of the experiment. Then assuming that is correct, does α_i have any value other than a free parameter? α_i was the major factor that brought the experiments and model into an agreement, is this fit general for the atmosphere or system specific?

Response:

The dynamic reconstruction of α_i is not produced by fitting SOA simulation with α_i to the smog chamber data. The dynamic α_i is created by compositing the two α_i sets at the fresh gas composition (fresh α_i) and the highly aged gas composition (highly aged α_i). The fresh α_i and the highly aged α_i are predicted using the predetermined equations, which are a function of NO_x level near the summer solstice (June 14th, 2018). At a given NO_x level, dynamic α_i is reconstructed using the aging scale factors ($f_A(t) = log\frac{[HO_2]+[RO_2]}{[HC]_0}$). Under a given NO_x level (HC ppbC/NO_x ppb) the $f_A(t)$ is maximized late afternoon (~4 PM) at near solstice. For the fresh condition, $f_A(fresh)$ is determined at 20% of total hydrocarbon consumption. $f_A(fresh)$ and $f_A(higly\ aged)$ are $f_A(t)$ values at fresh and highly aged conditions, respectively. For example, $f_A(fresh)$ and $f_A(higly\ aged)$ at HC/NO_x = 45 for toluene are -3.7 and -2.9, respectively. At HC/NO_x = 2, $f_A(fresh)$ and $f_A(higly\ aged)$ are -7.2 and -5.2, respectively. We define aging factor ($f_A{'}(t)$) at time = t as follows

$$f_A'(t) = \frac{f_A(highly\,aged) - f_A(t)}{f_A(highly\,aged) - f_A(fresh)}$$

Then, the α_i set is dynamically reconstructed by a weighted average method (Eq. (2) in the manuscript) using fresh α_i set, highly aged α_i set. and $f_A'(t)$.

In order to provide better description, Section 3.1 ("Atmospheric evolution of lumping species") has been revised and reads now,

"…The weighting factor at time = t is related to an aging scale factor ($f_A(t)$), which is defined as

$f_A(t) = log\frac{[HO_2]+[RO_2]}{[HC]_0}$,

(1)

where $[RO_2]$ and $[HO_2]$ represent the concentrations (ppb) of RO_2 and HO_2 radicals, respectively, and $[HC]_0$ represents the initial HC concentration (ppbC). The lower boundary of $f_A(t)$ (t = fresh) to determine the α_i set is equal to -7.2 at HC/NO_x=2 (high NO_x levels) and -3.7 at HC/NO_x=14 (low NO_x levels) for all three HCs. The upper value of $f_A(t)$ (t = highly aged) to determine the highly aged α_i set is equal to -5.2 and -2.9 under the same high and low NO_x levels, respectively. Both the fresh α_i and highly aged α_i are functions of HC/NO_x. $f_A(t)$ is further converted into a fractional aging scale ($f_A'(t)$) ranging from 0 (fresh composition) to 1 (highly-aged composition) using a weight average method ($f_A'(t) = \frac{f_A(highly\ aged) - f_A(t)}{f_A(highly\ aged) - f_A(fresh)}$) at each NO_x level. Then, α_i is dynamically reconstructed based on $f_A'(t)$ under varying NO_x conditions.

$\alpha_i = (1 - f_A'(t))(\text{fresh } \alpha_i) + (f_A'(t))(\text{highly aged } \alpha_i)$

(2)

…"

Minor Comments:

(1) Page 1 line 13: "applied to estimate" would be clearer if changed to "used to estimate"

Response:

This has been corrected in the revised manuscript.

(2) Page 1 line 19: Shouldn't the importance of electrolytes over NO_x or α_i, be expected or is this new insight?

Response:

The impact of hygroscopic seed, NO_x, or aging on SOA growth has been studied by numerous researchers. However, the relative importance of these variables on SOA was not well investigated. Based on our chamber studies and simulation results (Figure 7), we conclude that the effect of an aqueous phase containing electrolytes on SOA yields was more important than that of the NO_x level under our simulated conditions or the utilization of the age-driven α_i set.

(3) Page 1 line 21 and Page 11 line 14: "presence of wet electrolytic seeds" is this mainly the salting-in effect (and not chemical reactions) that causes the increase in SOA mass? From, Figure 7 the small fraction of OM_{AR} in A-D seems to suggest that is the case. Have you run simulations at higher RHs, say 90%?

Response:

Although some compounds (e.g., glyoxal) can be salting in (Kampf et al., 2013). In general, electrolytic inorganic salts results in salting out for most organic compounds (Wang et al., 2014). In this paper, the organic solubility in the salted aqueous phase was predicted using the predetermined polynomial equation, which was produced using the solubility (activity coefficient) of a variety of model compounds, which were parameterized with molecular weight (MW) and organic to carbon ratio (O:C) at different humidity and inorganic compositions. Evidently, the activity coefficient of most organic compound increases as increasing salt concentrations (decreasing humidity) supporting a salting out effect (Section S3 in supporting information). The sign of the coefficient for humidity in equation 4 is negative. In the revision of the manuscript, equation 4 was updated by including more model compounds and reads now,

$$\gamma_{in,i} = e^{4.789 \cdot ln(MW_i) - 4.701 \cdot ln(O{:}C_i) - 5.484 \cdot FS - 0.098 \cdot (100 \cdot RH) - 12.464}$$

(4) Page 4 line 10: There are theoretical calculations to include in the support the assumption of phase separation. See Zuend, A. and Seinfeld, J. H.: Modeling the gas-particle partitioning of secondary organic aerosol: The importance of liquid-liquid phase separation, Atmos. Chem. Phys., 12(9), 3857–3882, doi:10.5194/acp-12-3857-2012, 2012.

Response:

We cited the original paper in the manuscript at page 4 line 11.

(5) Page 5 line 26: How did you settle on this formula for the activity coefficients? I suggest adding that discussion to the SI.

Response:

In order to provide better description, Section S3 ("Activity coefficient of organic species in the aqueous phase containing electrolytes") has been revised and reads now,

"In the UNIAPR model, the formation of aromatic SOA is simulated with the assumption of organic-inorganic phase separation. To predict the partitioning of organic species on both the organic phase and the inorganic phase, the key model parameters are $K_{or,i}$ and $K_{in,i}$, respectively (described in Section 3.2 of the main manuscript). In order to predict $K_{in,i}$, the calculation of the activity coefficient ($\gamma_{in,i}$) of organic species in the inorganic phase (aqueous phase containing electrolytes) is necessary.

In our study, $\gamma_{in,i}$ was semi-empirically predicted by a polynomial equation, which was fit the theoretical $\gamma_{in,i}$ of various organic compounds to relative humidity (RH), fractional sulfate (FS), and molecular structures (i.e., molecular sizes (MW_i) and polarity ($O{:}C_i$)). The theoretical $\gamma_{in,i}$ was determined at the maximum solubility of organic species in the electrolytic aqueous phase (SO_4^{2-}-NH_4^+-H_2O system) using the Aerosol Inorganic-Organic Mixtures Functional Groups Activity Coefficients (AIOMFAC) (Zuend et al., 2011). AIOMFAC was run for the estimation of $\gamma_{in,i}$ of 26 model compounds with diverse MW_i and $O{:}C_i$ under varying inorganic phase compositions (FS and hygroscopicity linked to RH). The oligomeric products form in aqueous phase, but they deposit to the organic phase due to their poor solubility in inorganic phase. However, some hydrophilic oligomers can dissolve in both organic and inorganic phases. For example, glyoxal-origin oligomers might be hydrophilic and partially soluble in inorganic phase. Hence, the trace amount of glyoxal-oligomer (MW = 290 g/mol and O:C = 1 with mole fraction = 0.01) was included in inorganic phase as seen in Table S4. In Figure S1, the $\gamma_{in,i}$ predicted by AIOMFAC was plotted to that predicted by the polynomial equation (Eq. 4 in the manuscript) along with the one-to-one line for 26 organic species (Table S4). FS ranges from 0.34 to 1.0 and RH ranges from 0.1 to 0.8."

Table S4: The molecular structures of the oligomeric compound (a) and 26 model compounds (b) with O:C ratios and MW, which were employed to derive the polynomial equation to predict $\gamma_{in,i}$ of organic species in electrolytic aqueous phase. The name of the organic compound with symbol * originates from MCM website (http://mcm.leeds.ac.uk/MCMv3.3.1/home.htt).

(a)

#	Oligomer
Structure	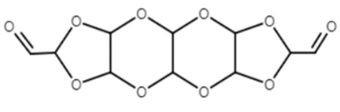
# of GLY	n=5
Formula	$C_{10}H_{10}O_{10}$ (n=5, nonhydrate on both end)
O:C	1.000
MW	290

(b)

#	1	2	3	4	5	6	7
Structure	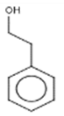	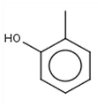		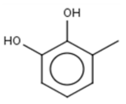		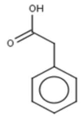	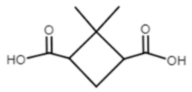
Name	phenethyl alcohol	o-cresol	2-methoxy-2-methylpropane	MCATECHOL*	1,7-heptanediol	phenylacetic acid	norpinic acid
Formula	C8H10O	C7H8O	C5H12O	C7H8O2	C7H16O2	C8H8O2	C8H12O4
O:C	0.125	0.143	0.200	0.286	0.286	0.250	0.500
MW	122.167	108.140	88.150	124.139	132.203	136.150	172.180

#	8	9	10	11	12	13	14
Structure	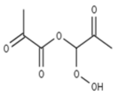	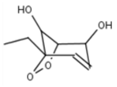	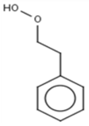	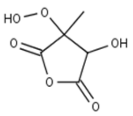	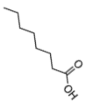	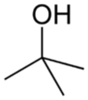	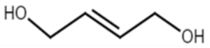
Name	C6OTKETOOH*	EBZBPER2OH*	2-phenylethylhydroperoxide	MMALNHYOOH*	octanoic acid	tert-butanol	1,4-dihydroxy-2-butene
Formula	C6H8O6	C8H12O4	C8H10O2	C5H6O6	C8H16O2	C4H13O	C4H8O2
O:C	1.000	0.500	0.250	1.200	0.250	0.250	0.500
MW	176.124	172.180	138.166	162.097	144.214	77.147	88.106

#	15	16	17	18	19	20	21
Structure	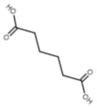		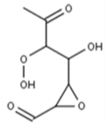	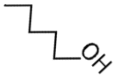	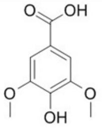	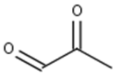	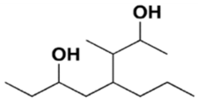
Name	hexanedioic acid	octanol	TLEMUCOOH*	1-pentanol	syringic acid	methylglyoxal	3-methyl-4-propyl-octane-2,6-diol
Formula	C6H10O4	C8H18O	C7H10O6	C5H12O	C9H10O5	C3H4O2	C12H26O2
O:C	0.667	0.125	0.857	0.200	0.556	0.667	0.167
MW	146.142	130.231	190.151	88.150	198.174	72.063	202.338

#	22	23	24	25	26
Structure	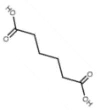	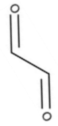	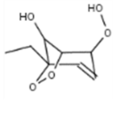	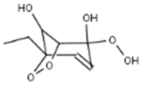	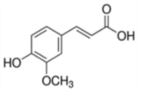
Name	1-propanol	glyoxal	EBZBPEROOH*	EBENZOLOOH*	ferulic acid
Formula	C3H8O	C2H2O2	C8H12O5	C8H12O6	C10H10O4
O:C	0.333	1.000	0.625	0.750	0.400
MW	60.096	58.000	188.179	204.178	194.186

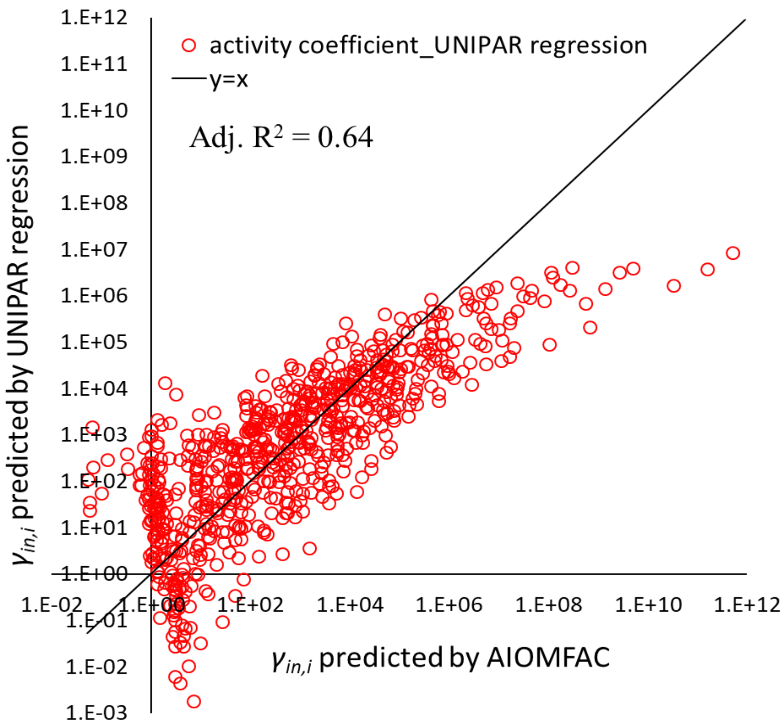

Figure S1: The $\gamma_{in,i}$ predicted by AIOMFAC was plotted to that predicted by the polynomial equation (Eq. 4 in the manuscript) along with the one to one line.

(6) Page 11 Line 3: "RH is insignificant" only at these experimental conditions. Maybe change to "RH is insignificant for our experiments, discussed in Section 4.2."

Response:

We changed the sentence to "… the effect of RH on SOA growth is insignificant in our simulation, discussed in Section 4.2."

(7) Figure 5: I find the figure's y-axis labels a bit cramped. Add a little more white space between the three panels to improve readability.

Response:

Figure 5 has been revised based on the comment the reviewer as follows,

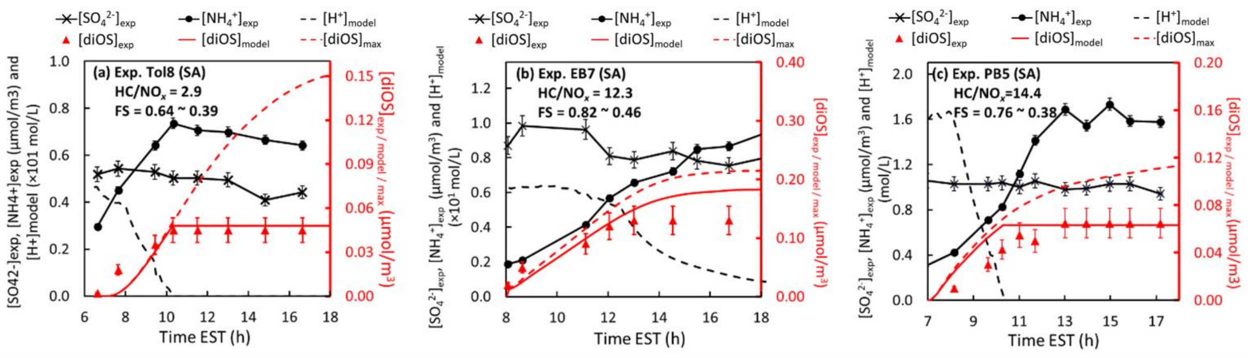

Figure 5: Time profiles of measured inorganic sulfate concentration ($[SO_4^{2-}]_{exp}$), ammonium concentration ($[NH_4^+]_{exp}$), diOS concentration ($[diOS]_{exp}$), the predicted proton concentration ($[H^+]$), diOS concentration ($[diOS]_{model}$), and the maximum diOS concentration ($[diOS]_{max}$) (assuming there is no ammonia neutralization in the system) for SOA generated from (a) toluene (HC/NO$_x$ = 2.9, OM-to-sulfate mass ratio (OM:sulf) = 1.4), (b) ethylbenzene (HC/NO$_x$ = 12.3, OM:sulf = 1.4), and (c) n-propylbenzene (HC/NO$_x$ = 14.4, OM:sulf = 0.7). The degree of neutralization is indicated by FS, which is ranging from 1 (for sulfuric acid) to 0.33 (for ammonium sulfate). "SA" stands for experiment with direct-injection sulfuric acid seeded aerosols. The ion and diOS concentrations were corrected for the particle loss to the chamber wall. The experimental conditions are available in Table 1.

Reference

Kampf, C. J., Waxman, E. M., Slowik, J. G., Dommen, J., Pfaffenberger, L., Praplan, A. P., Prévôt, A. S. H., Baltensperger, U., Hoffmann, T., and Volkamer, R.: Effective Henry's Law Partitioning and the Salting Constant of Glyoxal in Aerosols Containing Sulfate, Environmental Science & Technology, 47, 4236-4244, 10.1021/es400083d, 2013.

Wang, C., Lei, Y. D., Endo, S., and Wania, F.: Measuring and Modeling the Salting-out Effect in Ammonium Sulfate Solutions, Environmental Science & Technology, 48, 13238-13245, 10.1021/es5035602, 2014.

Zuend, A., Marcolli, C., Booth, A. M., Lienhard, D. M., Soonsin, V., Krieger, U. K., Topping, D. O., McFiggans, G., Peter, T., and Seinfeld, J. H.: New and extended parameterization of the thermodynamic model AIOMFAC: calculation of activity coefficients for organic-inorganic mixtures containing carboxyl, hydroxyl, carbonyl, ether, ester, alkenyl, alkyl, and aromatic functional groups, Atmospheric Chemistry and Physics, 11, 9155-9206, 10.5194/acp-11-9155-2011, 2011.

Reviewer 2

Interactive comment on “Simulation of SOA Formation from the Photooxidation of Monoalkylbenzenes in the Presence of Aqueous Aerosols Containing Electrolytes under Various NO_x Levels” by Chufan Zhou et al.

Chufan Zhou, Myoseon Jang, and Zechen Yu
mjang@ufl.edu

Received and published: 9 February 2019

We appreciate the reviewer for the valuable comments.

Major comments:

(1) It is unclear which experiments were conducted in sunlight, and how this important factor affected the results. The paper mentions that the sunlight from one experiment performed near summer solstice was used in gas-phase simulations, apparently for all experiments, even those conducted in mid-winter. Were all experiments performed on clear days? How might using more intense sunlight in simulations of winter experiments affect the uncertainties of the results?

Response:

Please also find the response to the major comment from reviewer 1. All the simulations were performed by using natural sunlight. As described in Section 3.1 in the manuscript, the aging scale factor is defined as $f_A(t) = log\frac{[HO_2]+[RO_2]}{[HC]_0}$. In order to set the aging scale factor for the fresh ($f_A(fresh)$) and highly aged processing ($f_A(higly\ aged)$) of hydrocarbon oxidation, we utilized the sunlight intensity near summer solstice (on 06/14/2018 with a clear sky in Gainesville, Florida (29.64185° N, 82.347883° W)). The aging factor ($f_A{}'(t)$) at time = t is estimated by using the equation below,

$$f_A{}'(t) = \frac{f_A(highly\ aged) - f_A(t)}{f_A(highly\ aged) - f_A(fresh)}$$

Then, the α_i set is dynamically reconstructed by a weighted average method (Eq. (2) in the manuscript) using fresh α_i set, highly aged α_i set and $f_A{}'$(t).

(2) p. 6 line 10: Was oligomerization in both the organic phase and the aqueous (inorganic) phase based on self-dimerization of individual products, or lumped products? In other words, were cross-reactions possible between molecules lumped into a single bin?

Response:

In UNIPAR model, oligomerization of organic compounds is processed in both the organic and the inorganic phases based on the self-dimerization reaction of lumped products. The cross-reactions between lumped species are complex. If highly reactive organic species react with weakly reactive species, this oligomerization may be less than the reaction of highly reactive organic species in a single bin but greater than the reaction of weakly reactive organic species in a single bin. Ultimately, they can be compensated in the production of organic matter. Thus, oligomerization in UNIAPR was treated as self-dimerization of lumped products within a single bin (Jang et al., 2005;Jang et al., 2006).

(3) p. 10 line 32: The authors identify a large temperature effect on SOA yields, as seen in other studies. However, the authors are uniquely positioned to identify whether this effect is due only to partitioning, as typically assumed, or is also due to temperature dependent reactions that either destroy condensable species or produce other species that hinder gas-to-particle transfers. Partitioning seems to be such a minor SOA source in this study that it is surprising that the observed temperature effects are so pronounced. Could the authors probe the cause of the temperature effect?

Response:

Gaseous lumped species first partitions onto aerosols based on a traditional gas-particle partitioning theory. In UNIAPR, the oligomerizations rate is processed by a second order reaction as follows.

$$\frac{dC_{or,i}}{dt} = -k_{o,i}{C'_{or,i}}^{2}\left(\frac{MW_i OM_T}{\rho_{or}\, 10^3}\right), \qquad \text{(Eq. 6 in the manuscript)}$$

$$\frac{dC_{in,i}}{dt} = -k_{AC,i}{C'_{in,i}}^{2}\left(\frac{MW_i M_{in}}{\rho_{in}\, 10^3}\right), \qquad \text{(Eq. 7 in the manuscript)}$$

The oligomerization rate constants (L mol^{-1} s^{-1}) in the organic (*or*) phase and inorganic (*in*) phase are $k_{o,i}$ and $k_{AC,i}$, respectively. The bracketed terms in the equations are the conversion factors from aerosol-base concentrations ($C'_{or,i}$ and $C'_{in,i}$: mol L^{-1}) into air-base concentrations (μg m^{-3}) (Section S5). ρ_{or} and ρ_{in} represent the density of the *or* and *in* aerosol. The concentrations (μg m^{-}

^{3} of air) of species i in the gas phase ($C_{g,i}$), *or* phase ($C_{or,i}$) and *in* phase ($C_{in,i}$) are estimated using partitioning coefficients in the multiphase: i.e., $K_{or,i}$ (m^3 μg^{-1}, g /*or*) and $K_{in,i}$ (m^3 μg^{-1}, g /*in*). $K_{or,i}$ and $K_{in,i}$ are calculated (by Pankow(Pankow, 1994)) by using estimated activity coefficients in the *or* and *in* phase ($\gamma_{or,i}$ and $\gamma_{in,i}$), the mass concentration of media (OM_T and M_{in}), and vapor pressure (p_i°) (See Section 3.3 SOA formation: aerosol-phase reactions). If $C_{or,i}$ and $C_{in,i}$ increase, the formation of oligomerization also increases. Numerous studies have shown that a large fraction of SOA is oligomers (Tolocka et al., 2004;Loeffler et al., 2006;Hoffer, 2004;Baltensperger et al., 2005;Hastings et al., 2005;Riva et al., 2019).

(4) In Figure 5, dialkyl organosulfates (diOS) concentrations seem to track ammonium concentrations. In one experiment, the authors comment that diOS formation ceases when the aerosol effloresces. Is there any causative relationship between diOS and ammonium concentrations in wet aerosol?

Response:

When acidity is high in wet aerosol, both the diOS formation and the neutralization of acidic sulfate with ammonia can occur. When the inorganic phase is effloresced (no aqueous phase), organic compounds cannot be dissolved in the inorganic phase. Generally, the neutralization of acidic sulfate with ammonia in wet aerosol is faster than OS formation. When the gaseous ammonia concentration is high, sulfuric acid will be consumed by ammonia and thus the formation of diOS can be less. The formation of diOS depends on the concentrations of both acidic sulfate and reactive organic species in the aerosol phase. The prediction of the diOS formation ($[diOS]_{model}$) is performed using the semiempirical equation derived previously for several SOA systems such as aromatic and isoprene SOA (Im et al., 2014;Beardsley and Jang, 2016) as follows,

$$\frac{[diOS]_{model}}{[SO_4^{2-}]_{free}} = 1 - \frac{1}{1 + f_{diOS}\frac{N_{diOS}}{[SO_4^{2-}]_{free}}}, \qquad \text{(Eq. 9 in the manuscript)}$$

N_{diOS} represents the numeric parameter originating from the quantity of reactive chemical species available to form diOS. This parameter is near-explicitly predicted in the model. f_{diOS} represents the semi-empirically determined diOS conversion factor using various chamber data. At each time step, acidic free sulfate ($[SO_4^{2-}]_{free}$), which is the sulfate that is unassociated with ammonium

($[NH_4^+]$), is estimated as ($[SO_4^{2-}] - 0.5\ [NH_4^+]$) and applied to estimate $[diOS]_{model}$. As seen in the equation above, diOS formation ($\frac{[diOS]_{model}}{[SO_4^{2-}]_{free}}$) is not linearly related to $[SO_4^{2-}]_{free}$. Generally, the high proton concentration ($[H^+]$) in the aerosol indicates the high concentration of $[SO_4^{2-}]_{free}$ available for diOS formation. In the morning when humidity is high (>80%), gaseous ammonia concentrations are low because they are condensed on the chamber wall. The ammonia concentrations rise in daytime when humidity is low because ammonia is off-gassing from the chamber wall. Hence, the formation rate of diOS decreases by the two reasons: (1) the consumption of $[SO_4^{2-}]_{free}$ due to diOS formation and (2) the neutralization of $[SO_4^{2-}]_{free}$ with gaseous ammonia as shown in Figure 5 (flat diOS curve in the afternoon).

(5) Figure 7 implies that in most experiments, aqueous-phase SOA production is much greater than SOA production via traditional partitioning mechanisms, but the authors don't seem to make this comparison or comment on it. Is it a fair comparison?

Response:

The traditional partitioning-based SOA models such as two products model (Odum et al., 1996) or several semivolatile surrogates model (e.g., volatility basis set (VBS)) (Donahue et al., 2006) utilizes semiempirical parameters (e.g., the product stoichiometric coefficient (α) and gas-particle partitioning coefficient (K_p)) for each HC system under a given NO_x condition. The parameters in traditional partitioning-base models are apparently fit to observed SOA mass. Although the theory facilitates the predicting of SOA mass in the absence of inorganic seed, the SOA mass from the traditional surrogate-based partitioning models is not truly partitioning mass. In UNIAPR, OM_P is predicted solely by the partitioning theory using a near-explicit molecular structure with their activity coefficient and vapor pressure and thus OM_P will be less than the mass prediction using a traditional surrogate-based partitioning models.

(6) Figure S1 indicates that ozone is generated too quickly in the model, sometimes by a factor of 2 or 3. Can the authors comment on the implications of this overprediction? Is it related to the "artificial OH radicals" added to the model in certain experiments?

Response:

The over-prediction of ozone is not due to an artificial OH radical. As shown in the Figure below, ozone is over-predicted by removing make-up of artificial OH radicals. However, both the addition of artificial OH radicals and overestimation of ozone indicate potential problems in MCM for oxidation of monoalkylbenzenes. The MCM developers and other researchers also reported over-prediction of ozone for aromatic photooxidation (Bloss et al., 2005;Wagner et al., 2003). We have performed numerous chamber experiments. The overestimation of ozone using MCM appears in monoalkylbenzene series, while a good agreement between predictions and observations is found in xylenes, and trimethylbenzenes, terpenes and isoprene. We propose several explanations for the deviation of predicted ozone formation from the observations.

(a) RO_2 chemistry in MCM mechanisms is still uncertain. Numerous products and reactions are involved to form RO_2. The cross-reactions between RO_2 and the reaction of various RO_2 with HO_2 are complex (Villenave et al., 1998;Jokinen et al., 2014). Oversimplified surrogate coefficients for the diverse RO_2 chemistry could trigger the discrepancy between the modeled and the measured OH radical concentration.

(b) In the gas kinetic mechanism, the photolysis rate constants of organic compounds were also oversimplified using surrogate compounds and can cause uncertainty in ozone prediction and production distributions.

(c) The recent laboratory investigation shows the significance of gas-wall partitioning of organic compounds. The loss of oxygenated products to the chamber wall can lead the lower ozone measurements than the model prediction.

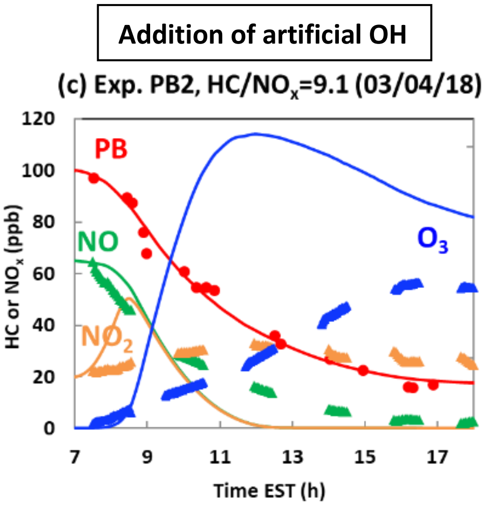
Addition of artificial OH

(c) Exp. PB2, HC/NO_x=9.1 (03/04/18)

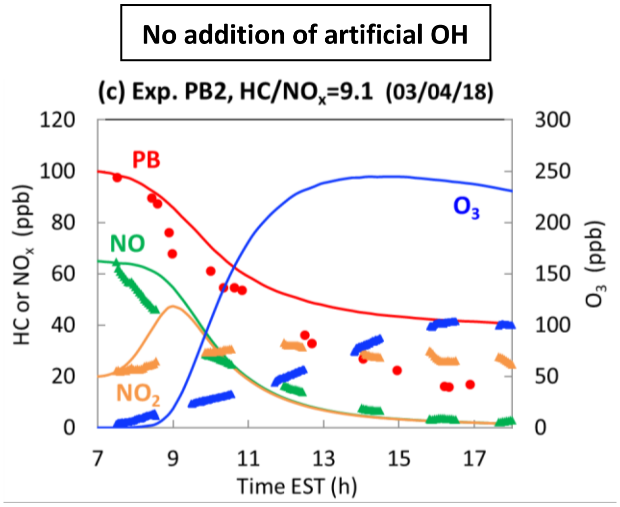
No addition of artificial OH

(c) Exp. PB2, HC/NO_x=9.1 (03/04/18)

Minor comments:

(1) p. 2 line 5: Unclear comparison: "… fewer global emissions" that what?

Response:

We changed the sentence to "…, despite fewer global emissions compared with biogenic VOCs."

(2) p. 2 line 11: When the authors refer to "regional weather" do they really mean climate change? p. 4 line 9: unclear comparison with literature: What system was "the reported value of 2" measured for? Is it a toluene oxidation study?

Response:

p. 2 line 11: We referred to climate change. We changed the sentence to "SOA formation has attracted substantial interest from scholars because of its vital role in affecting climate change, …"

p. 4 line 9: It is measure from a series of toluene oxidation study. We changed the sentence to "The ratio of organic matter (OM) to OC was experimentally determined to be 1.9 (Table 1, EB4), the reported value of 2 for a series of toluene-NO_x oxidation study (Kleindienst et al., 2007)."

(3) p. 6 line 18: another unclear comparison with literature: What system was "the reported value of 1.4 g/cm^3" measured for?

Response:

We changed the sentence to "ρ_{or} and ρ_{in} represent the density of the aerosol of *or* and *in* aerosol. ρ_{or} was experimentally determined (EB4 in Table 1) to be 1.38 g cm^{-3}, which was similar to the reported value of 1.4 g/cm^3 for aromatic SOA (Ng et al., 2007;Nakao et al., 2011;Chen et al., 2017)."

(4) p. 7 line 2: It appears that "irreversibility and nonvolatility" should be "irreversibly formed and nonvolatile".

Response:

This has been corrected in the revised manuscript.

(5) p. 9 line 12: The meaning of the phrase "contributed to" is unclear in this sentence.

Response:

We changed the sentence to "… In this study, aromatic SOA mass is attributed to a few highly reactive species, such as GLY…"

Reference

Baltensperger, U., Kalberer, M., Dommen, J., Paulsen, D., Alfarra, M. R., Coe, H., Fisseha, R., Gascho, A., Gysel, M., Nyeki, S., Sax, M., Steinbacher, M., Prevot, A. S. H., Sjögren, S., Weingartner, E., and Zenobi, R.: Secondary organic aerosols from anthropogenic and biogenic precursors, Faraday Discuss, 130, 265, 10.1039/b417367h, 2005.

Beardsley, R. L., and Jang, M.: Simulating the SOA formation of isoprene from partitioning and aerosol phase reactions in the presence of inorganics, Atmospheric Chemistry and Physics, 16, 5993-6009, 10.5194/acp-16-5993-2016, 2016.

Bloss, C., Wagner, V., Jenkin, M. E., Volkamer, R., Bloss, W. J., Lee, J. D., Heard, D. E., Wirtz, K., Martin-Reviejo, M., Rea, G., Wenger, J. C., and Pilling, M. J.: Development of a detailed chemical mechanism (MCMv3.1) for the atmospheric oxidation of aromatic hydrocarbons, Atmospheric Chemistry and Physics, 5, 641-664, DOI 10.5194/acp-5-641-2005, 2005.

Chen, L. H., Bao, K. J., Li, K. W., Lv, B., Bao, Z. E., Lin, C., Wu, X. C., Zheng, C. H., Gao, X., and Cen, K. F.: Ozone and Secondary Organic Aerosol Formation of Toluene/NOx Irradiations under Complex Pollution Scenarios, Aerosol Air Qual Res, 17, 1760-1771, 10.4209/aaqr.2017.05.0179, 2017.

Donahue, N. M., Robinson, A. L., Stanier, C. O., and Pandis, S. N.: Coupled partitioning, dilution, and chemical aging of semivolatile organics, Environmental Science & Technology, 40, 2635-2643, 10.1021/es052297c, 2006.

Hastings, W. P., Koehler, C. A., Bailey, E. L., and De Haan, D. O.: Secondary organic aerosol formation by glyoxal hydration and oligomer formation: Humidity effects and equilibrium shifts during analysis, Environmental Science & Technology, 39, 8728-8735, 2005.

Hoffer, A.: Chemical characterization of humic-like substances (HULIS) formed from a lignin-type precursor in model cloud water, Geophys Res Lett, 31, 10.1029/2003gl018962, 2004.

Im, Y., Jang, M., and Beardsley, R. L.: Simulation of aromatic SOA formation using the lumping model integrated with explicit gas-phase kinetic mechanisms and aerosol-phase reactions, Atmospheric Chemistry and Physics, 14, 4013-4027, 10.5194/acp-14-4013-2014, 2014.

Jang, M., Czoschke, N. M., Northcross, A. L., Cao, G., and Shaof, D.: SOA formation from partitioning and heterogeneous reactions: Model study in the presence of inorganic species, Environmental Science & Technology, 40, 3013-3022, 10.1021/es0511220, 2006.

Jang, M. S., Czoschke, N. M., and Northcross, A. L.: Semiempirical model for organic aerosol growth by acid-catalyzed heterogeneous reactions of organic carbonyls, Environmental Science & Technology, 39, 164-174, 10.1021/es048977h, 2005.

Jokinen, T., Sipilä, M., Richters, S., Kerminen, V.-M., Paasonen, P., Stratmann, F., Worsnop, D., Kulmala, M., Ehn, M., Herrmann, H., and Berndt, T.: Rapid Autoxidation Forms Highly Oxidized RO 2 Radicals in the Atmosphere, 53, 14596-14600, 10.1002/anie.201408566, 2014.

Kleindienst, T. E., Jaoui, M., Lewandowski, M., Offenberg, J. H., Lewis, C. W., Bhave, P. V., and Edney, E. O.: Estimates of the contributions of biogenic and anthropogenic hydrocarbons to secondary organic aerosol at a southeastern US location, Atmospheric Environment, 41, 8288-8300, 10.1016/j.atmosenv.2007.06.045, 2007.

Loeffler, K. W., Koehler, C. A., Paul, N. M., and De Haan, D. O.: Oligomer formation in evaporating aqueous glyoxal and methyl glyoxal solutions, Environmental Science & Technology, 40, 6318-6323, 2006.

Nakao, S., Clark, C., Tang, P., Sato, K., and Cocker, D.: Secondary organic aerosol formation from phenolic compounds in the absence of NOx, Atmospheric Chemistry and Physics, 11, 10649-10660, 10.5194/acp-11-10649-2011, 2011.

Ng, N. L., Kroll, J. H., Chan, A. W. H., Chhabra, P. S., Flagan, R. C., and Seinfeld, J. H.: Secondary organic aerosol formation from m-xylene, toluene, and benzene, Atmospheric Chemistry and Physics, 7, 3909-3922, DOI 10.5194/acp-7-3909-2007, 2007.

Odum, J. R., Hoffmann, T., Bowman, F., Collins, D., Flagan, R. C., and Seinfeld, J. H.: Gas/particle partitioning and secondary organic aerosol yields, Environmental Science & Technology, 30, 2580-2585, Doi 10.1021/Es950943+, 1996.

Pankow, J. F.: An absorption model of the gas/aerosol partitioning involved in the formation of secondary organic aerosol, Atmos. Environ., 28, 189-193, 1994.

Riva, M., Heikkinen, L., Bell, D. M., Peräkylä, O., Zha, Q., Schallhart, S., Rissanen, M. P., Imre, D., Petäjä, T., Thornton, J. A., Zelenyuk, A., and Ehn, M.: Chemical transformations in monoterpene-derived organic aerosol enhanced by inorganic composition, npj Climate and Atmospheric Science, 2, 10.1038/s41612-018-0058-0, 2019.

Tolocka, M. P., Jang, M., Ginter, J. M., Cox, F. J., Kamens, R. M., and Johnston, M. V.: Formation of Oligomers in Secondary Organic Aerosol, Environmental Science & Technology, 38, 1428-1434, 10.1021/es035030r, 2004.

Villenave, E., Lesclaux, R., Seefeld, S., and Stockwell, W. R.: Kinetics and atmospheric implications of peroxy radical cross reactions involving the CH3C(O)O2radical, Journal of Geophysical Research: Atmospheres, 103, 25273-25285, 10.1029/98jd00926, 1998.

Wagner, V., Jenkin, M. E., Saunders, S. M., Stanton, J., Wirtz, K., and Pilling, M. J.: Modelling of the photooxidation of toluene: conceptual ideas for validating detailed mechanisms, Atmospheric Chemistry and Physics, 3, 89-106, 10.5194/acp-3-89-2003, 2003.

Simulation of SOA Formation from the Photooxidation of Monoalkylbenzenes in the Presence of Aqueous Aerosols Containing Electrolytes under Various NO_x Levels

Chufan Zhou, Myoseon Jang, and Zechen Yu

Department of Environmental Engineering Sciences, University of Florida, Gainesville, 32611, USA

Correspondence to: Myoseon Jang (mjang@ufl.edu)

Abstract. The formation of secondary organic aerosols (SOAs) from the photooxidation of three monoalkylbenzenes (toluene, ethylbenzene, and n-propylbenzene) in the presence of inorganic seeds (SO_4^{2-}-NH_4^+-H_2O system) under varying NO_x levels has been simulated using the Unified Partitioning-Aerosol Phase Reaction (UNIPAR) model. The evolution of the volatility-reactivity distribution (mass-base stoichiometric coefficient, α_i) of oxygenated products, which were created by the near-explicit gas kinetic mechanism, was integrated with the model using the parameters linked to the concentrations of HO_2 and RO_2 radicals. This dynamic distribution was used to estimate the model parameters related to the thermodynamic constants of the products in multiple phases (e.g., the gas phase, organic phase, and inorganic phase) and the reaction rate constants in the aerosol phase. The SOA mass was predicted through the partitioning and aerosol chemistry processes of the oxygenated products in both the organic phase and aqueous solution containing electrolytes, with the assumption of organic-inorganic phase separation. The prediction of the time series SOA mass (12-hr), against the aerosol data obtained from an outdoor photochemical smog chamber, was improved by the dynamic α_i set compared to the prediction using the fixed α_i set. Overall, the effect of an aqueous phase containing electrolytes on SOA yields was more important than that of the NO_x level under our simulated conditions or the utilization of the age-driven α_i set. Regardless of the NO_x conditions, the SOA yields for the three aromatics were significantly higher in the presence of wet electrolytic seeds than those obtained with dry seeds or no seed. When increasing the NO_x level, the fraction of organic matter (OM) produced by aqueous reactions to the total OM increased due to the increased formation of relatively volatile organic nitrates and peroxyacyl nitrate like products. The predicted partitioning mass fraction increased as the alkyl chain length increases but the organic mass produced via aerosol phase reactions decreased due to the increased activity coefficient of the organic compounds containing longer alkyl chains. Overall, the lower mass-base SOA yield was seen in the longer alkyl-substituted benzene in both the presence and absence of inorganic seeded aerosols. However, the difference of mole-base SOA yields of three monoalkylbenzenes becomes small because the highly reactive organic species (i.e., glyoxal) mainly originates from ring opening products without alkyl side chain. UNIPAR predicted the conversion of hydrophilic, acidic sulfur species to non-electrolytic dialkyl-organosulfate (diOS) in the aerosol.

Deleted: applied

Thus, the model predicted the impact of diOS on both hygroscopicity and acidity, which subsequently influenced aerosol growth via aqueous reactions.

1 Introduction

Anthropogenic volatile organic compounds (VOCs) have significant impacts on urban and regional atmospheric chemistry, despite fewer global emissions compared with biogenic VOCs (McDonald et al. (2018). As an important group of anthropogenic VOCs, aromatic hydrocarbons (HCs) are emitted from automobile exhaust (Zhang et al., 2018) and solvent use Cheng et al. (2018) and are known to be precursors for secondary organic aerosols (SOAs), which are formed during the process of photooxidation (Seinfeld and Pandis, 2016). In polluted areas (e.g., urban areas in Asia), aromatic HCs occupy 11 % to 25 % of the total nonmethane HC emissions (67.0 Tg in 2010) (Li et al., 2017) and traditionally comprise approximately 15 % of SOA formation (Ait-Helal et al., 2014), which contributes to the urban budget of fine particulate matter (Wood et al., 2010).

Deleted: .

SOA formation has attracted substantial interest from scholars because of its vital role in affecting climate change (IPCC, 2015;Seinfeld and Pandis, 2016), urban visibility (Chen et al., 2012;Ren et al., 2018), and health (Requia et al., 2018). The prediction of SOA formation was first fulfilled by a gas-particle partitioning model. The partitioning-based SOA model uses two surrogate products (Odum et al., 1996) or several semivolatile surrogates (e.g., volatility basis set (VBS)) (Donahue et al., 2006), with semiempirical parameters (e.g., the product stoichiometric coefficient (α) and gas-particle partitioning coefficient (K_p)) for each HC system under a given NO_x condition. Due to its simplicity and high efficiency, the partitioning-base model has been widely used in regional and global models. Nonetheless, the models and their predecessors are limited to predict SOAs formed from in-particle chemistry due to the loss of product structures, which govern the reactivity of organic species in the aerosol phase. Overall, regional air quality models have historically underestimated fine particulate matter in summertime (Appel et al., 2017;Huang et al., 2017) due to the lack of in-particle chemistry, particularly in the presence of an aqueous phase containing electrolytes (Ervens et al., 2011;Tsigaridis et al., 2014;Kelly et al., 2018).

Deleted: regional weather

A few models have attempted to implement in-particle chemistry into SOA models. For instance, Johnson et al. (2004) (2005) simulated aromatic SOA chamber data, with a modified K_p, to obtain experimentally comparable results, while the delayed simulated SOA mass indicated the occurrence of chemical reactions in the aerosol phase. McNeill et al. (2012) developed the Gas Aerosol Model for Mechanism Analysis (GAMMA) to predict the formation of SOAs via aqueous phase chemistry, which was further applied to the production of isoprene SOAs. Im et al. (2014) advanced the Unified Partitioning-Aerosol Phase Reaction (UNIPAR) model, which predicted the SOA mass from partitioning processes and aerosol-phase reactions (reactions in both organic and inorganic phases and organosulfate (OS) formation). In that study, toluene and 1,3,5-trimethylbenzene SOAs were modeled using near-explicit products with the organic-inorganic phase separation mode. Beardsley and Jang (2016) extended UNIPAR to simulate isoprene SOAs in the single homogeneously mixed phase (organic-inorganic mixture). Despite the reasonable prediction of SOA masses, UNIPAR faced inaccuracies in predicting time series SOA data due to the use of a fixed (nonage-driven) mass-based stoichiometric coefficient (α_i) set.

Age-driven functionalization and fragmentation alter the volatility and reactivity of products and their molecular structures (Donahue et al., 2006;Rudich et al., 2007;Shilling et al., 2007;Hartikainen et al., 2018) which, in turn, varies the in-particle chemistry. Cappa and Wilson (2012) employed tunable parameters to kinetically demonstrate the evolution of SOA mass and the bulk oxygen-to-carbon atomic ratio (O:C ratio) during photochemical aging. However, oligomerization reactions in the aerosol phase were excluded. Donahue et al. (2011) developed a 2D-VBS method, which represented product aging by remapping the volatility and polarity (O:C ratio) of the products in 2D space. Zhao et al. (2015) reported a discrepancy in the simulated toluene SOAs and α-pinene SOAs within the same 2D-VBS configuration, which may result from the different reactivities of the oxidation products of the precursors in aerosol-phase reactions. In this study, we have attempted to improve the UNIPAR model by using dynamic (age-driven) α_i and applying the resulting model to predict the SOA formation of three monoalkylbenzenes (i.e., toluene, ethylbenzene, and n-propylbenzene) under a wide range of environmental conditions (i.e., NO_x, temperature, humidity, sunlight and aerosol acidity). To consider the effect of the aging process on SOA formation, model parameters related to the organic molecular structures (i.e., the molecular weight (MW) and O:C ratio) and the α_i set are calculated as the system ages, allowing for the internally dynamic estimation of the activity coefficient of the products (lumping species) in the aqueous phase containing electrolytes. Hence, the model is able to dynamically compute the partitioning coefficient of organics in the inorganic phase (K_{in}) by reflecting the photochemical evolution of the products in the gas phase and, consequently, improving SOA prediction. Organosulfate (OS), which has been identified in both laboratory and field studies (Hettiyadura et al., 2015;Li et al., 2016a;Estillore et al., 2016;Chen et al., 2018), is an important chemical species due to its low volatility and ability to modulate the hygroscopicity of sulfate constituents. In the presence of acidic sulfate constituents, UNIPAR also predicts the production of non-electrolytic sulfates (i.e., dialkyl-substituted OS (diOS)) and the ensuing modification of aqueous phase reactions. The feasibility of unified rate constants for aerosol-phase reactions was evaluated by extending the preexisting rate constants, which has been employed for toluene and 1,3,5-trimethylbenzene (Im et al., 2014) and isoprene (Beardsley and Jang, 2016), to the three monoalkylbenzenes in this study.

2 Experimental techniques

The SOA formation from the photooxidation of monoalkylbenzenes were conducted in the University of Florida Atmospheric PHotochemical Outdoor Reactor (UF-APHOR) (Table 1). The concentrations of HCs, trace gasses (NO_x, SO_2, and O_3), inorganic ions, aerosol acidity and organic carbon (OC) of particles were monitored, as were the meteorological factors (i.e., relative humidity (RH), temperature, and ultraviolet (UV) radiation). The configurations of the chamber and instrumentations were described by Im et al. (2014), Li et al. (2016a), Beardsley and Jang (2016), Yu et al. (2017), and Jiang et al. (2017).

Aerosol acidity ([H^+], mol/L of aerosol) is monitored using colorimetry integrated with the reflectance UV-visible spectrometer (C-RUV) technique (Li et al. (2015a)) (Section S4 in the supporting information (SI)). The diOS concentration (μmol m^{-3}) in an aerosol is estimated by the difference [H^+] obtained from ion chromatography (IC) interfaced with a particle-into-liquid sampler (PILS) (Li et al. (2015a) and C-RUV method. Each HC was studied under at least two NO_x levels (high NO_x: HC/NO_x < 5.5; low NO_x: HC/NO_x > 5.5) with or without inorganic seeded aerosols (i.e., sulfuric acid (SA) or ammonium sulfate (AS)). HONO was added into the system as a reaction initiator. To investigate the effect of the liquid water content (LWC) on AS seeded SOA, two RH conditions were applied. (1) dry: RH < efflorescence RH (ERH) of the AS seed; (2) wet: RH > 50 % to prevent crystallization of AS seed. The ratio of organic matter (OM) to OC was experimentally determined to be 1.9 (Table 1, EB4), which was similar to the reported value of 2.0 for a series of toluene-NO_x oxidation study (Kleindienst et al., 2007).

3 Model descriptions

The structure of the UNIPAR model is illustrated in Fig. 1. The simulation of aromatic SOA formation in the aqueous phase containing electrolyte was performed under the assumption of complete organic-inorganic phase separation. Bertram et al. (2011) modeled the separation RH (SRH) in the liquid-liquid phase of the mixture of organic and AS using the bulk O:C ratio. When ambient RH < SRH, the system undergoes organic-inorganic phase separation. The reported O:C ratios of the toluene, ethylbenzene, and n-propylbenzene SOAs were 0.62 (Sato et al., 2012), 0.55 (Sato et al., 2012), and 0.45 (Li et al., 2016b), respectively, which caused the corresponding SRH values to be 65 %, 80 %, and 93 %, respectively. Most RH for active photooxidation of HCs under ambient sunlight were under 65%, which supported the assumption of organic-inorganic phase separation. In addition, as less soluble oligomers formed in the aerosol phase, an SRH higher than 65 % was more likely to be yielded.

3.1 Atmospheric evolution of lumping species

The gas-phase oxidation of HCs is simulated using the near-explicit gas-phase chemistry mechanism (Master Chemical Mechanism (MCM) v 3.3.1) (Jenkin et al., 2012) integrated with the Morpho chemical solver (Jeffries et al., 1998). To represent the polluted urban and clean environments, the gas-phase oxidation is simulated under various NO_x levels (HC ppbC/NO_x ppb=2 - 14) for given meteorological conditions (e.g., sunlight, temperature, and RH on 06/14/18 near the summer solstice, with a clear sky in Gainesville, Florida). The resulting oxygenated products are lumped into 51 species within a 2D set with 8 levels of volatility (1-8: 10^{-8}, 10^{-6}, 10^{-5}, 10^{-4}, 10^{-3}, 10^{-2}, 10^{-1}, and 1 mmHg) and 6 levels of aerosol-phase reactivity (very fast: VF, fast: F, medium: M, slow: S, partitioning only: P, and multi-alcohol: MA) plus 3 additional reactive species (glyoxal (GLY), methylglyoxal (MGLY), and epoxydiols (IEPOX, isoprene products)) with own vapour pressure. The detailed lumping criteria and α_i equations are described in Section S1 in the SI along with the major product structures (Tables S1-S3).

To simulate age-dependent SOA formation, α_i is reconstructed over time by a weighted average method using a pair of gas-phase oxidation compositions with different aging statuses: fresh composition and highly oxidized composition. The weighting factor at time = t is related to an aging scale factor ($f_A(t)$) which is defined as

$$f_A(t) = log\frac{[HO_2]+[RO_2]}{[HC]_0}, \tag{1}$$

where [RO$_2$] and [HO$_2$] represent the concentrations (ppb) of RO$_2$ and HO$_2$ radicals, respectively, and [HC]$_0$ represents the initial HC concentration (ppbC). The lower boundary of $f_A(t)$ (t = fresh) to determine the α_i set is equal to -7.2 at HC/NO$_x$=2 (high NO$_x$ levels) and -3.7 at HC/NO$_x$=14 (low NO$_x$ levels) for all three HCs. The upper value of $f_A(t)$ (t = highly aged) to determine the highly aged α_i set is equal to -5.2 and -2.9 under the same high and low NO$_x$ levels, respectively. Both the fresh α_i and highly aged α_i are functions of HC/NO$_x$. $f_A(t)$ is further converted into a fractional aging scale ($f_A{}'(t)$) ranging from 0 (fresh composition) to 1 (highly-aged composition) using a weight average method ($f_A{}'(t) = \frac{f_A(highly\ aged) - f_A(t)}{f_A(highly\ aged) - f_A(fresh)}$) at each NO$_x$ level. Then, α_i is dynamically reconstructed based on $f_A{}'(t)$ under varying NO$_x$ conditions.

$$\alpha_i = (1 - f_A{}'(t))(\text{fresh } \alpha_i) + (f_A{}'(t))(\text{highly aged } \alpha_i) \tag{2}$$

The molecular structures, including $O:C_i$ and MW (MW_i), of each species (i) are also dynamically represented by a similar method, as shown in the SI in Section S2.

3.2 SOA formation: partitioning

The partitioning coefficient (K_P) from the gas (g) phase to the organic (or) phase ($K_{or,i}$, m^3 µg^{-1}) and from the g phase to the inorganic (in) phase ($K_{in,i}$, m^3 µg^{-1}) of each species is estimated using the following gas-particle absorption model (Pankow, 1994).

$$K_{or,i} = \frac{7.501\ R\ T}{10^9\ MW_{or}\ \gamma_{or,i}\ p^0_{l,i}} \quad \text{and} \quad K_{in,i} = \frac{7.501\ R\ T}{10^9\ MW_{in}\ \gamma_{in,i}\ p^0_{l,i}}, \tag{3}$$

where R represents the gas constant (8.314 J mol^{-1} K^{-1}). T represents the ambient temperature (K). MW_{or} and MW_{in} represent the average MW (g mol^{-1}) of organic and inorganic aerosols, respectively. $p^0_{l,i}$ represents the subcooled liquid vapor pressure (mmHg) of a species, i. In the or phase, we assume that the activity coefficient ($\gamma_{or,i}$) of a species (i) is unity (Jang and Kamens, 1998). In the in phase, $\gamma_{in,i}$ is semi-empirically predicted by a regression equation, which was fit the theoretical activity coefficients of various organic compounds to RH, fractional sulfate (FS), and molecular structures (i.e., MW_i and $O:C_i$). FS is a numerical indicator for inorganic compositions related to aerosol acidity ($FS = \frac{[SO_4^{2-}]}{[SO_4^{2-}]+[NH_4^+]}$, where $[SO_4^{2-}]$ and $[NH_4^+]$ are the concentration of the total sulfate and the total ammonium, respectively). The theoretical activity coefficients were estimated at a given humidity and an aerosol composition through a thermodynamic model (Aerosol Inorganic-Organic Mixtures Functional Groups Activity Coefficients (AIOMFAC)) (Zuend et al., 2011).

$$\gamma_{in,i} = e^{4.789\cdot ln(MW_i) - 4.701\cdot ln(O:C_i) - 5.484\cdot FS - 0.098\cdot(100\cdot RH) - 12.464} \tag{4}$$

Deleted: t

Deleted: (t)

Deleted:),

Deleted: boundaries

Deleted: (t)

Deleted: t

Deleted: fresh

Deleted: of fresh composition

Deleted:).

Deleted: boundary

Deleted: (t)

Deleted: t

Deleted: α_i set for

Deleted: composition is obtained when f_A

Deleted: (t)

Deleted: factor, $f_A{}'$,

Deleted: -

Deleted: (0: fresh composition; 1: highly aged composition).

Deleted:

The statistical information for Eq. 4 is shown in the SI in Section S3 and Fig. S1. The resulting $K_{or,i}$ and $K_{in,i}$ are employed to calculate the concentration (µg m^{-3}) of the lumping species in multiple phases ($C_{g,i}$, $C_{or,i}$, $C_{in,i}$, and $C_{T,i} = C_{g,i} + C_{or,i} + C_{in,i}$). Schell et al. (2001) developed a partitioning model to predict SOA formation. This model was reconstructed by Cao and Jang (2010) to include OM formed via aerosol-phase reactions ($OM_{AR,i}$) for a species (i), which is estimated in Section 3.3. OM formed during the partitioning process (OM_P) is estimated by utilizing the mass balance shown in the following equation.

$$OM_P = \sum_{ij}\left[C_{T,i} - OM_{AR,i} - \; C^*_{g,i}\,\frac{\frac{C_{or,i}}{MW_i}}{\sum_{ij}(\frac{C'_{or,i}}{MW_i} + \frac{OM_{AR,i}}{MW_{oli,i}}) + OM_0}\right] \tag{5}$$

$C^*_{g,i}$ $(1/K_{or,i})$ is the effective saturation concentration and OM_0 represents the concentration (mol m^{-3}) of the preexisting OM. $MW_{oli,i}$ represents the average MW of oligomeric products. Eq. 5 is solved via iterations using the globally converging Newton-Raphson method (Press et al., 1992).

3.3 SOA formation: aerosol-phase reactions

The formation of $OM_{AR,i}$ is processed in both *or* and *in* phases: oligomerization in the *or* phase to form $OM_{AR,or,i}$ and oligomerization in the *in* phase to form $OM_{AR,in,i}$ based on the assumption of a self-dimerization reaction (i.e., second-order reaction) (Odian, 2004) for organic compounds in media. Oligomerization in an aqueous phase can be accelerated under acidic environment (Jang et al., 2002). The oligomerization rate constants (L mol^{-1} s^{-1}) in the *or* phase and *in* phase are $k_{o,i}$ and $k_{AC,i}$, respectively, and the kinetic equations for oligomerizations are written as follows.

$$\frac{dC_{or,i}}{dt} = -k_{o,i}{C'_{or,i}}^{2}(\frac{MW_i OM_T}{\rho_{or}\,10^3})), \tag{6}$$

$$\frac{dC_{in,i}}{dt} = -k_{AC,i}{C'_{in,i}}^{2}(\frac{MW_i M_{in}}{\rho_{in}\,10^3})), \tag{7}$$

The bracketed terms in the equations indicate the conversion factors from aerosol-base concentrations ($C'_{or,i}$ and $C'_{in,i}$: mol L^{-1}) into air-base concentrations (µg m^{-3}). The detailed derivations are shown in Section S5 and are illustrated in Fig. S2. ρ_{or} and ρ_{in} represent the density of the aerosol of *or* and *in* aerosol. ρ_{or} was experimentally determined (EB4 in Table 1) to be 1.38 g cm^{-3}, which was similar to the reported value of 1.4 g cm^{-3} for aromatic SOA (Nakao et al., 2011;Chen et al., 2017). ρ_{in} is obtained from a regression equation through the extended aerosol inorganic model (E-AIM)(Clegg et al., 1998). Due to atmospheric diurnal patterns (high RH at nighttime to low humidity during daytime), it is likely that the RH changes would be based on inorganic aerosol ERH. UNIPAR internally predicts the ERH using the equation derived by Colberg et al. (2003).

$k_{AC,i}$ in Eq. 7 is estimated based on a semiempirical model developed by Jang et al. (2005) as a function of species reactivity (R_i), protonation equilibrium constant ($pK_{BH^+_i}$), excess acidity (X), water activity (a_w), and proton concentration ([H$^+$]), which are estimated by the E-AIM.

$$k_{AC,i} = 10^{1.3R_i + 0.0005\,pK_{BH^+_i} + 1.3\cdot X + log\left(a_w[H^+]\right) - 5.5} \tag{8}$$

In the *or* phase, $k_{o,i}$ is estimated by excluding the X and $a_w\,[H^+]$ terms. The formed OM_{AR} can be calculated as a sum of $OM_{AR,or,i}$ and $OM_{AR,or,i}$ for each species assuming that OM_{AR} is irreversibly formed and nonvolatile (Kleindienst et al., 2006;Cao and Jang, 2010).

Deleted: irreversibility

Deleted: nonvolatility

3.4 Organosulfate formation

In the presence of aqueous acidic sulfate, UNIPAR predicts the formation of diOS ($[diOS]_{model}$) to compute the change in aerosol hygroscopicity and acidity. At each time step, free electrolytic sulfate ($[SO_4^{2-}]_{free}$), which is the sulfate that is unassociated with ammonium ($[NH_4^+]$), is represented as ($[SO_4^{2-}] - 0.5\,[NH_4^+]$). $[SO_4^{2-}]_{free}$ is then applied to the semiempirical equation tested previously for several SOA systems (Im et al., 2014;Beardsley and Jang, 2016) to predict $[diOS]_{model}$, as described below,

$$\frac{[diOS]_{model}}{[SO_4^{2-}]_{free}} = 1 - \frac{1}{1 + f_{diOS}\frac{N_{diOS}}{[SO_4^{2-}]_{free}}}, \qquad (9)$$

where f_{diOS} represents the diOS conversion factor introduced by Im et al. (2014), which was semi-empirically determined to be 0.063 in this study. N_{diOS} represents the numeric parameter for scaling lumping groups based on the effectiveness of the chemical species to form diOS. For example, the diOS scale factor is 1 for each alcohol and aldehyde group and 2 for each epoxide group (see Tables S1-S3 for functional groups). Then, N_{diOS} is summed at each time step and applied to Eq. 9.

3.5 Operation of the UNIPAR model

The variables, which include HC consumption (ΔHC), [HO_2], [RO_2], HC/NO_x, RH, temperature, and the inorganic concentration (i.e., Δ[SO_4^{2-}] and Δ[NH_4^+]), were input to the UNIPAR model every 6 minutes (Δt=6 minutes).

4 Results and discussion

4.1 Prediction of SOA mass under the evolution of oxygenated products

As reported in former studies, the kinetic mechanism tends to underestimate the decay of aromatic HCs because of the low prediction of OH radicals (Johnson et al., 2005;Bloss et al., 2005). In this study, the addition of artificial OH radicals varies with the HC/NO_x ratio by fitting the predicted decay of HCs using the kinetic mechanism in the experimental measurements. The time profiles of the decays of the three HCs are shown in Fig. S3 in the SI. When the NO_x level is very low, the maximum additional OH radical production rate for monoalkylbenzenes is 2×10^8 molecules $cm^3\ s^{-1}$, which is less than 4×10^8 (Bloss et al., 2005) but similar to the value reported by Im et al. (2014). When HC/NO_x < 3, no addition of artificial OH radicals is needed for the chamber simulation of the decay of monoalkylbenzenes. For the make-up OH production rate constants of all three HCs under varying NO_x, the mathematical weighting equation is written below,

$$dynamic\ makeup\ OH\ rate = \frac{e^{0.6\times HC/NO_x}}{e^{0.6\times HC/NO_x}+50} \times 2.0 \times 10^8 \text{ molecules cm}^3\text{ s}^{-1} \qquad (10)$$

In our model, we assume that the oxidation of products progresses in the gas phase. Lambe et al. (2012) reported that the transition point of n-C_{10} SOAs from a functionalization dominant regime to a fragmentation dominant regime is approximately 3 days (photochemical equivalent age under an atmospheric OH exposure of 1.5×10^6 molecules cm^{-3}). Under this criterion, we exclude the aging of nonvolatile aerosol products (OM_{AR}). However, the oxidation of aerosol products for longer periods of time may decrease the volatility (George and Abbatt, 2010;Jimenez et al., 2009).

Fig. 2 illustrates the evolution of the volatility-reactivity-based distribution of the mass-based stoichiometric coefficient (α_i) of toluene at the two different NO_x levels (HC/NO_x=2.9 and 10.5). Collectively, most α_i values at both NO_x levels tend to decline as the reaction time lapses (Fig. 2(a) vs. Fig. 2(b); Fig. 2(c) vs. Fig. 2(d)) since the evolution of some semivolatile organic compounds (SVOCs) forms very volatile molecules (i.e., CO_2, formic acid, and formaldehyde). For example, the α_i values of highly reactive carbonyls with high volatility (GLY and MGLY in Table S1) are high under the fresh condition and significantly decline as the system ages, because they undergo fast photolysis under sunlight (George et al., 2015;Henry and Donahue, 2012). Consequently, the decay of these highly reactive species leads to the decrease in the production of OM_{AR}. The high NO_x level delays the oxidation of gas-phase products. Similar trends in the α_i set can be found for ethylbenzene and n-propylbenzene, as shown in Fig. S4 (Table S2) and Fig. S5 (Table S3), respectively. The α_i of highly reactive species (e.g., GLY, 8VF, 3M, and 5S) decreases by increasing the NO_x level due to the suppression of the HO_x cycle via the reaction of NO_2 with OH radicals. As seen in Fig. 2(d), some medium reactivity species (i.e., 2-methyl-4-oxo-3-nitro-2-butenoic acid (3M), 2-methyl-4-oxo-2-butenoic acid (6M), and acetyl-3-oxopropanoate (7M)) start to form as NO_x decreased.

In Fig. 3, the comparison between the simulations of SOA formation from toluene oxidation is based on two different α_i-reconstruction strategies: dynamic α_i and fixed α_i. A clear improvement in the prediction of SOA formation is demonstrated when comparing the SOA mass using dynamic α_i to that using fixed α_i. The aged SOA growth from the three systems (i.e., low NO_x level (Fig. 3(a) and Fig. 3(d)), moderate NO_x level (Fig. 3(b) and Fig. 3(e)), and high NO_x level with an inorganic seed (Fig. 3(c) and Fig. 3(f)) are even smaller than that predicted with the less-aged α_i set, which is fixed at the time of the HCs being consumed half of the total consumption. Our model simulation against the chamber data suggests that while aging may alter aerosol compositions (Fig. 2), it does not always increase SOA yields. Traditionally, the SOA mass has been predicted using fixed thermodynamic parameters (i.e., K_p and α_i), which is inadequate when reflecting upon practical scenarios, where oxygenated product distributions vary dynamically with oxidation.

4.2 Effects of aerosol acidity and LWC on SOA formation

In the model, aerosol acidity was expressed using a fractional free sulfate (FFS), which is defined as FFS=($[SO_4^{2-}]$ - $0.5[NH_4^+]$)/$[SO_4^{2-}]$. Humidity can influence both aerosol acidity and LWC, which are the model parameters in UNIPAR. Thus, UNIPAR has the capability to decouple the effect of aerosol acidity and humidity, as shown in Fig. 4 for toluene SOA. The impact of aerosol acidity and humidity on the yields of SOAs derived from ethylbenzene and n-propylbenzene is illustrated in

Fig. S6. The dramatic difference in SOA yields appears between the RH above ERH and the RH below ERH. The LWC disappears below ERH, and there are no aqueous reactions. For example, the observed SOA yield of ethylbenzene with effloresced AS was significantly smaller than that with wet AS: 11 % (EB8 in Table 1) vs. 30 % (EB9 in Table 1). Kamens et al. (2011) and Liu et al. (2018) reported a significantly lower yield of toluene SOA for dry AS seeded aerosols compared with its wet counterpart. The partitioning of polar carbonaceous products increases with increasing LWC and, thus, aqueous reactions. In the presence of wet aerosols, SOA yields gradually increase with increasing FFS (increasing acidity) at a given RH due to acid-catalyzed oligomerization. The oxygenated products of toluene are relatively more polar than those of ethylbenzene or propylbenzene and positively attribute to increase of OM_{AR}.

Compared to isoprene SOAs reported by Beardsley and Jang (2016), the impacts of humidity and acidity on the SOA yields of monoalkylbenzenes in this study are relatively weaker above the ERH (Fig. 4), except for the highly acidic conditions under high humidity. In this study, aromatic SOA mass is attributed to a few highly reactive species, such as GLY. Other aromatic oxidation products partitioned in the aerosol phase have moderate solubility and they are slow to react in the aqueous phase. Isoprene products are more hygroscopic than aromatic products and even mixable with an aqueous phase containing electrolytes. The reactions of medium reactivity polar products that formed during isoprene oxidation can be accelerated by an acid catalyst with higher sensitivities to acidity and humidity.

Deleted: The formation of

Deleted: SOAs

Deleted: contributed

4.3 Organosulfate: simulation vs. measurement

Fig. 5 illustrates the time profiles of the predicted concentrations of diOS ($[diOS]_{model}$) and protons ($[H^+]$) with the measured concentrations of diOS ($[diOS]_{exp}$), $[NH_4^+]$, and $[SO_4^{2-}]$ for different aromatic HCs under given experimental conditions (Fig. 5(a)-(c)). For the three SA seeded SOA experiments, the fractions of diOS to the total sulfate amount are 0.09, 0.15, and 0.06 for toluene (Exp. Tol8, HC/NO_x=2.9, FS changing from 0.64 to 0.39), ethylbenzene (Exp. EB7, HC/NO_x=12.3, FS changing from 0.82 to 0.46), and n-propylbenzene (Exp. PB5, HC/NO_x=14.4, FS changing from 0.76 to 0.38), respectively. The $[diOS]_{model}$ reasonably agrees with $[diOS]_{exp}$. The aerosols in Exp. Tol8 and Exp. PB5 show the cease in diOS formation at approximately 10 am since they became effloresced due to the neutralization of SA with ammonia under the reduction in humidity during the daytime. The diOS fraction in Exp. EB7, which contained wet acidic aerosols, was higher than those in Exp. Tol8 and Exp. PB5 indicating that the acidic condition was favorable for the formation of diOS (Surratt et al., 2010;Lin et al., 2013).

Beardsley and Jang (2016) reported that the diOS fraction for isoprene SOAs was 0.26 (HC/NO_x=32.5, FS changing from 0.69 to 0.47), which was more than that for toluene SOAs, indicating that the oxidation products of isoprene may contain more reactive species to form diOS. For example, IEPOX products in isoprene SOAs are known to be reactive to SA (Budisulistiorini et al., 2017). Additionally, isoprene aerosol products are mixable with aqueous solutions containing electrolytes, and they can more effectively form diOS compared to the aromatic products in liquid-liquid phase separation.

To estimate the potential upper boundary of the concentration of diOS ($[diOS]_{max}$) in monoalkylbenzene SOA, the aerosol composition was predicted by the model in the presence of SA aerosols (without neutralization with ammonia) under the given experimental conditions shown in Fig. 5. The resulting diOS fractions were 0.29 (OM-to-sulfate mass ratio (OM:sulf) = 1.4), 0.25 (OM:sulf = 1.4), and 0.12 (OM:sulf = 0.7) for toluene, ethylbenzene and n-propylbenzene, respectively. The aerosol acidity of the ambient aerosol is generally lower than ammonium hydrogen sulfate (AHS) and, thus, the diOS fraction in ambient air would be much lower than the estimated upper boundary. Fig. 5 suggests that the change in both aerosol acidity and hygroscopicity by the formation of nonelectrolytic sulfate is important to predict SOA mass.

4.4 Effect of NO_x on SOA formation in the presence of an aqueous phase containing electrolytes

Fig. 6 shows the impact of NO_x on the three aromatic SOAs in this study by producing SOAs at two different NO_x levels in the presence and absence of SO_2. Overall, regardless of the inorganic seed conditions, both the chamber observation and model simulation suggest that increasing the NO_x level leads to the decreased formation of SOAs. This trend in the absence of inorganic seed aerosols has also been observed multiple times (Li et al., 2015;Ng et al., 2007;Song et al., 2005). By increasing NO_x, the path of an RO_2 radical progresses to the formation of organonitrate and peroxyacyl nitrate (PAN) products, which are less reactive to aerosol-phase reactions. They are relatively volatile and, thus, insignificantly attribute to partitioning SOA mass.

For example, the SOA yields under the low NO_x level (HC(ppbC)/NO_x(ppb)=9.1~14.8, Table 1) in the presence of SO_2, with a similar degree of ammonia titration (i.e., similar FS values by the end of the experiments), were higher than those without seeded aerosols: 42 % for toluene (Exp. Tol1, FS=0.44), 26 % for ethylbenzene (Exp. EB1, FS=0.37), and 66 % for propylbenzene (Exp. PB1, FS=0.43). The impact of aerosol acidity was even greater for SOAs produced under a high NO_x level (HC(ppbC)/NO_x(ppb)=2.8~5.0): 65 % for toluene (Exp. Tol3, FS=0. 43), 146 % for ethylbenzene (Exp. EB5, FS=0. 39), and 77 % for propylbenzene (Exp. PB3, FS=0. 40). SOA formation under high NO_x conditions is generally more sensitive to aerosol acidity compared to that at low NO_x levels (Figs. 6(a)-(c) and Fig. S7(f) vs. Figs. 6(d)-(f)). The fractions of medium reactivity products are relatively high in high NO_x levels and their reactions in aerosol phase can be accelerated by an acid catalyst.

4.5 Sensitivity of SOA formation to humidity, temperature, aerosol acidity, precursor HCs, and NO_x level

Fig. 7 illustrates the sensitivity of the SOA mass simulated at relatively low concentration of HC (20 ppb) (panel I) for three monoalkylbenzenes to important variables (i.e., humidity (A-I vs. B-I for AHS and C-I vs. D-I for AS), temperature (A-I vs. E-I for AHS and F-I vs. G-I without inorganic aerosol), aerosol acidity (A-I vs. C-I at RH=45 % and B-I vs. D-I at RH=65 %), and NO_x levels (A-I vs. H-I with AHS seeded aerosols and F-I vs. I-I without inorganic seeded aerosols)). The most drastic change appears by changing the temperature from 273 K (E-I) to 298 K (A-I). The SOA yield is known to increase by 20-150

%, which results from a 10 K decrease in temperature (Sheehan and Bowman, 2001). For all SOAs, noticeable changes are shown between the absence (F-I) and presence (A-I) of wet inorganic seeds, while a minor change appears between wet AHS (A-I) and wet AS (C-I). Within the wet acidic aerosols (A-I vs. B-I and C-I vs. D-I), the effect of RH is insignificant in our simulation, as discussed in Section 4.2. Although the impact of NO_x (A-I vs. H-I and F-I vs. I-I) is less than that of temperature and inorganic seeds, SOA yields are still significantly altered, as discussed in Section 4.4.

Panel II series in Fig. 7 illustrates SOA growth curves under various conditions shown in panel I. Overall, the simulated SOA yields (slopes) increase with a decreased alkyl chain length (toluene > ethylbenzene > n-propylbenzene), which is consistent with our chamber observations (Table 1). Although the decreased of vapor pressure of products benefits increases in OM_P as the alkyl chain length increases, the increase of the activity coefficient of the organic products containing longer alkyl chains in aqueous phase is unfavorable to form OM_{AR} via aqueous reactions. However, the difference of mole-base SOA yields of three monoalkylbenzenes becomes small because the highly reactive organic species (i.e., glyoxal), which are produced through ring opening reactions without alkyl side chain, significantly attribute to OM_{AR}. Panel II confirms that the effect of an aqueous phase containing electrolytes on SOA yields is more critical than that of the NO_x level under our simulated conditions.

4.6 Sensitivity of model prediction to major variables and model uncertainty

To determine the model sensitivity to these parameters, simulations (Exp. Tol9 in Table 1) were performed by increasing/decreasing vapor pressure (V_p), the enthalpy of vaporization (H_{vap}), $\gamma_{in,i}$, and $k_{AC,i}$ by factors of 1.5, 1.1, 1.5, and 2, respectively. The corresponding changes in the SOA mass are 27.4 %/-20.1 %, 0.2 %/-0.1 %, 9.3 %/9.3 %, and 7.7 %/-8.22 %, respectively. The change in SOA mass from the baseline for each simulation is shown in Fig. S8.

The uncertainty associated with the group contribution method used for V_p estimation is a factor of 1.45 (Zhao et al., 1999). H_{vap} has a reported error of 2.6 % (Kolska et al., 2005). $\gamma_{in,i}$ is estimated as a function of O:C, MW, RH, and FS (Eq. 4). $k_{AC,i}$ is semi-empirically calculated based on $[H^+]$, LWC, and species reactivity (Eq. 8). The E-AIM is performed to estimate the LWC, which is reliable and based on a broadly used water activity dataset (Zhang et al., 2000). Yet, the inorganic thermodynamic models including E-AIM performed inadequately in the prediction of $[H^+]$ under low RH and ammonia rich conditions (FS < 0.55) (Li and Jang, 2012).

Although most identified toluene products have been included, such as methyl-cyclohexene (3S), 2-methyl-5-nitrophenol (5P), 2-methyl-benzoquione (6S), 2-methyl-4-oxo-2-butenoic acid (6M), o-cresol (7P), 3-hydroxy-1,3-propandial (7VF), 3-methyl-2(5H)-furanone (8P), MGLY, and GLY (Forstner et al., 1997;Jang and Kamens, 2001;Sato et al., 2007;Gomez Alvarez et al., 2007;Huang et al., 2016), a large amount of toluene oxidation mechanisms and involved products remain unstudied. A similar trend can be found in ethylbenzene and propylbenzene. Evidently, the addition of artificial OH radicals in the gas-phase simulation suggests missing mechanisms in the MCM v 3.3.1 or an improper branching ratio of reactions. Additionally, the diverse reactions of the RO_2 radicals might be oversimplified in the gas-phase simulation by employing surrogate coefficients. In the model, non-electrolytic diOS was predicted and applied to prediction of LWC and $[H^+]$, which subsequently affect aerosol growth via aqueous reactions. Typically, the monoalkyl sulfate is identified as a product of the esterification of SA with reactive species (Hettiyadura et al., 2015;Li et al., 2016a;Estillore et al., 2016;Chen et al., 2018). It is possible that monoalkyl sulfates can influence LWC and aerosol acidity differently from sulfuric acid, although they are strongly acidic and hygroscopic. Although Noziere et al. (2010) reported that OS could be produced by the reactions of GLY and sulfate radicals in the presence of aqueous AS under UV light, the amounts of formed monoalkyl OS and their influence on aerosol hygroscopicity is still not clear.

Some other factors in recent investigations, such as organic vapor wall loss and aerosol viscosity, have not accounted for by the UNIPAR model. The loss of organic vapor to the Teflon chamber wall can compete with the gas-particle partitioning process and the reactions in both the gas phase and aerosol phase to initiate a negative bias in the experimental measurements (Zhang et al., 2014;Mcvay et al., 2014). The modeling of the gas-wall process of semivolatile organic compounds can improve the prediction of SOA mass in regional scales. In addition, an increased aerosol viscosity via aging could modify the diffusivity of the partitioned organic molecules (Abramson et al., 2013) and the reaction rate constant for oligomerization in the aerosol phase.

5 Conclusions and implications

Despite numerous studies in SOA characterization and formation mechanisms, substantial biases between the simulated and field-measured SOA mass were still found (Hodzic et al., 2016) due to the inadequacy of handling the dynamic multigenerational aging (Jathar et al., 2016) and aqueous reactions of the oxygenated products in the presence of an aqueous phase containing electrolytes (Ervens et al., 2011). In this study, the UNIPAR model addressed those issues using a dynamic age-driven α_i set, multiphase partitioning of organic compounds, and in-particle chemistry. Although the utilization of the age-driven α_i set improves the time series prediction of SOA mass, as shown in Fig. 3, the photochemical evolution of the gas-phase products via monoalkylbenzene oxidation (Fig. 2, Fig. S4, and Fig. S5) does not increase the SOA mass, as is commonly suggested. Overall, the effect of an aqueous phase containing electrolytes on SOA formation was more critical than that of the NO_x level under our simulated conditions. By adding a wet inorganic seed to the non-seed SOA system, the mass-base SOA yields under high NO_x levels increase more than those under low NO_x conditions (Fig. 6 in Section 4.4). The vapor pressure of volatile organonitrate and PAN-like species, which are formed at high NO_x levels, are not low enough to increase partitioning SOA mass (Fig. 7 A-II). Thus, SOA yields decreased by increasing NO_x levels. Overall, both simulation and chamber data show that monoalkylbenzene SOA yields increase with a decreased alkyl chain length: toluene > ethylbenzene > n-propylbenzene. This difference is most noticeable in the presence of an inorganic seed at high NO_x levels (Fig. 7 A-II and H-II). (Colberg et al., 2003)

Due to the pervasiveness and relatively high concentration of toluene in the urban situation, where HC/NO_x < 5.5 and wet inorganic seeds typically exist, the importance of toluene SOAs to the urban SOA burden can increase. The oxidation products from aromatic HCs can also involve cloud condensation nuclei activity due to their high reactivity via heterogeneous chemistry (Molteni et al., 2018), resulting in a change in the properties of clouds and fog and the urban radiation balance (Gordon et al., 2016). The unified aerosol-phase reaction rate constants for three monoalkylbenzenes represent the feasibility of applying the UNIPAR model to more aromatic systems (dialkyl benzenes and trialkyl benzenes) and the complex urban mixture.

Author contribution. Jang designed the experiments and Zhou and Yu carried them out. Jang developed the model, and Zhou performed the calculation of model parameters and the simulations. Zhou and Jang prepared the manuscript with contributions from Yu.

Acknowledgments. This research was supported by the National Strategic Project-Fine particle of the National Research Foundation of Korea (NRF) funded by the Ministry of Science and ICT(MSIT), the Ministry of Environment (ME), and the Ministry of Health and Welfare (MOHW) (2017M3D8A1090654).

References

Abramson, E., Imre, D., Beranek, J., Wilson, J., and Zelenyuk, A.: Experimental determination of chemical diffusion within secondary organic aerosol particles, Phys Chem Chem Phys, 15, 2983-2991, 10.1039/c2cp44013j, 2013.

Ait-Helal, W., Borbon, A., Sauvage, S., de Gouw, J. A., Colomb, A., Gros, V., Freutel, F., Crippa, M., Afif, C., Baltensperger, U., Beekmann, M., Doussin, J. F., Durand-Jolibois, R., Fronval, I., Grand, N., Leonardis, T., Lopez, M., Michoud, V., Miet, K., Perrier, S., Prevot, A. S. H., Schneider, J., Siour, G., Zapf, P., and Locoge, N.: Volatile and intermediate volatility organic compounds in suburban Paris: variability, origin and importance for SOA formation, Atmospheric Chemistry and Physics, 14, 10439-10464, 10.5194/acp-14-10439-2014, 2014.

Appel, K. W., Napelenok, S. L., Foley, K. M., Pye, H. O. T., Hogrefe, C., Luecken, D. J., Bash, J. O., Roselle, S. J., Pleim, J. E., Foroutan, H., Hutzell, W. T., Pouliot, G. A., Sarwar, G., Fahey, K. M., Gantt, B., Gilliam, R. C., Heath, N. K., Kang, D. W., Mathur, R., Schwede, D. B., Spero, T. L., Wong, D. C., and Young, J. O.: Description and evaluation of the Community Multiscale Air Quality (CMAQ) modeling system version 5.1, Geosci Model Dev, 10, 1703-1732, 10.5194/gmd-10-1703-2017, 2017.

Beardsley, R. L., and Jang, M.: Simulating the SOA formation of isoprene from partitioning and aerosol phase reactions in the presence of inorganics, Atmospheric Chemistry and Physics, 16, 5993-6009, 10.5194/acp-16-5993-2016, 2016.

Bertram, A. K., Martin, S. T., Hanna, S. J., Smith, M. L., Bodsworth, A., Chen, Q., Kuwata, M., Liu, A., You, Y., and Zorn, S. R.: Predicting the relative humidities of liquid-liquid phase separation, efflorescence, and deliquescence of mixed particles of ammonium sulfate, organic material, and water using the organic-to-sulfate mass ratio of the particle and the oxygen-to-carbon elemental ratio of the organic component, Atmospheric Chemistry and Physics, 11, 10995-11006, 10.5194/acp-11-10995-2011, 2011.

Bloss, C., Wagner, V., Jenkin, M. E., Volkamer, R., Bloss, W. J., Lee, J. D., Heard, D. E., Wirtz, K., Martin-Reviejo, M., Rea, G., Wenger, J. C., and Pilling, M. J.: Development of a detailed chemical mechanism (MCMv3.1) for the atmospheric oxidation of aromatic hydrocarbons, Atmospheric Chemistry and Physics, 5, 641-664, DOI 10.5194/acp-5-641-2005, 2005.

Budisulistiorini, S. H., Nenes, A., Carlton, A. G., Surratt, J. D., McNeill, V. F., and Pye, H. O. T.: Simulating Aqueous-Phase Isoprene-Epoxydiol (IEPOX) Secondary Organic Aerosol Production During the 2013 Southern Oxidant and Aerosol Study (SOAS), Environmental Science & Technology, 51, 5026-5034, 10.1021/acs.est.6b05750, 2017.

Cao, G., and Jang, M.: An SOA Model for Toluene Oxidation in the Presence of Inorganic Aerosols, Environmental Science & Technology, 44, 727-733, 10.1021/es901682r, 2010.

Cappa, C. D., and Wilson, K. R.: Multi-generation gas-phase oxidation, equilibrium partitioning, and the formation and evolution of secondary organic aerosol, Atmospheric Chemistry and Physics, 12, 9505-9528, 10.5194/acp-12-9505-2012, 2012.

Chen, J., Zhao, C. S., Ma, N., Liu, P. F., Gobel, T., Hallbauer, E., Deng, Z. Z., Ran, L., Xu, W. Y., Liang, Z., Liu, H. J., Yan, P., Zhou, X. J., and Wiedensohler, A.: A parameterization of low visibilities for hazy days in the North China Plain, Atmospheric Chemistry and Physics, 12, 4935-4950, 10.5194/acp-12-4935-2012, 2012.

Chen, L. H., Bao, K. J., Li, K. W., Lv, B., Bao, Z. E., Lin, C., Wu, X. C., Zheng, C. H., Gao, X., and Cen, K. F.: Ozone and Secondary Organic Aerosol Formation of Toluene/NOx Irradiations under Complex Pollution Scenarios, Aerosol Air Qual Res, 17, 1760-1771, 10.4209/aaqr.2017.05.0179, 2017.

Chen, X., Xie, M. J., Hays, M. D., Edgerton, E., Schwede, D., and Walker, J. T.: Characterization of organic nitrogen in aerosols at a forest site in the southern Appalachian Mountains, Atmospheric Chemistry and Physics, 18, 6829-6846, 10.5194/acp-18-6829-2018, 2018.

Cheng, K., Hao, W.-W., Yi, P., Zhang, Y., and Zhang, J.-Y.: Volatile Organic Compounds Emission from Chinese Wood Furniture Coating Industry: Activity-based Emission Factor, Speciation Profiles, and Provincial Emission Inventory, Aerosol Air Qual Res, 10.4209/aaqr.2018.02.0044, 2018.

Clegg, S. L., Brimblecombe, P., and Wexler, A. S.: Thermodynamic model of the system $H^+ - NH_4^+ - SO_4^{2-} - NO_3^- - H_2O$ at tropospheric temperatures, The Journal of Physical Chemistry A, 102, 2137-2154, 1998.

Colberg, C. A., Luo, B. P., Wernli, H., Koop, T., and Peter, T.: A novel model to predict the physical state of atmospheric H2SO4/NH3/H2O aerosol particles, Atmospheric Chemistry and Physics, 3, 909-924, DOI 10.5194/acp-3-909-2003, 2003.

Donahue, N. M., Robinson, A. L., Stanier, C. O., and Pandis, S. N.: Coupled partitioning, dilution, and chemical aging of semivolatile organics, Environmental Science & Technology, 40, 2635-2643, 10.1021/es052297c, 2006.

Donahue, N. M., Epstein, S. A., Pandis, S. N., and Robinson, A. L.: A two-dimensional volatility basis set: 1. organic-aerosol mixing thermodynamics, Atmospheric Chemistry and Physics, 11, 3303-3318, 10.5194/acp-11-3303-2011, 2011.

Ervens, B., Turpin, B. J., and Weber, R. J.: Secondary organic aerosol formation in cloud droplets and aqueous particles (aqSOA): a review of laboratory, field and model studies, Atmospheric Chemistry and Physics, 11, 11069-11102, 10.5194/acp-11-11069-2011, 2011.

Estillore, A. D., Hettiyadura, A. P., Qin, Z., Leckrone, E., Wombacher, B., Humphry, T., Stone, E. A., and Grassian, V. H.: Water Uptake and Hygroscopic Growth of Organosulfate Aerosol, Environ Sci Technol, 50, 4259-4268, 10.1021/acs.est.5b05014, 2016.

Forstner, H. J. L., Flagan, R. C., and Seinfeld, J. H.: Secondary organic aerosol from the photooxidation of aromatic hydrocarbons: Molecular composition, Environmental Science & Technology, 31, 1345-1358, Doi 10.1021/Es9605376, 1997.

George, C., Ammann, M., D'Anna, B., Donaldson, D. J., and Nizkorodov, S. A.: Heterogeneous Photochemistry in the Atmosphere, Chem Rev, 115, 4218-4258, 10.1021/cr500648z, 2015.

George, I. J., and Abbatt, J. P. D.: Heterogeneous oxidation of atmospheric aerosol particles by gas-phase radicals, Nat Chem, 2, 713-722, 10.1038/nchem.806, 2010.

Gomez Alvarez, E., Viidanoja, J., Munoz, A., Wirtz, K., and Hjorth, J.: Experimental confirmation of the dicarbonyl route in the photo-oxidation of toluene and benzene, Environmental Science & Technology, 41, 8362-8369, 10.1021/es0713274, 2007.

Gordon, H., Sengupta, K., Rap, A., Duplissy, J., Frege, C., Williamson, C., Heinritzi, M., Simon, M., Yan, C., Almeida, J., Trostl, J., Nieminen, T., Ortega, I. K., Wagner, R., Dunne, E. M., Adamov, A., Amorim, A., Bernhammer, A. K., Bianchi, F., Breitenlechner, M., Brilke, S., Chen, X. M., Craven, J. S., Dias, A., Ehrhart, S., Fischer, L., Flagan, R. C., Franchin, A., Fuchs, C., Guida, R., Hakala, J., Hoyle, C. R., Jokinen, T., Junninen, H., Kangasluoma, J., Kim, J., Kirkby, J., Krapf, M., Kurten, A., Laaksonen, A., Lehtipalo, K., Makhmutov, V., Mathot, S., Molteni, U., Monks, S. A., Onnela, A., Perakyla, O., Piel, F., Petaja, T., Praplanh, A. P., Pringle, K. J., Richards, N. A. D., Rissanen, M. P., Rondo, L., Sarnela, N., Schobesberger, S., Scott, C. E., Seinfeldo, J. H., Sharma, S., Sipila, M., Steiner, G., Stozhkov, Y., Stratmann, F., Tome, A., Virtanen, A., Vogel, A. L., Wagner, A. C., Wagner, P. E., Weingartner, E., Wimmer, D., Winkler, P. M., Ye, P. L., Zhang, X., Hansel, A., Dommen, J., Donahue, N. M., Worsnop, D. R., Baltensperger, U., Kulmala, M., Curtius, J., and Carslaw, K. S.: Reduced anthropogenic aerosol radiative forcing caused by biogenic new particle formation, P Natl Acad Sci USA, 113, 12053-12058, 10.1073/pnas.1602360113, 2016.

Hartikainen, A., Yli-Pirila, P., Tiitta, P., Leskinen, A., Kortelainen, M., Orasche, J., Schnelle-Kreis, J., Lehtinen, K. E. J., Zimmermann, R., Jokiniemi, J., and Sippula, O.: Volatile Organic Compounds from Logwood Combustion: Emissions and Transformation under Dark and Photochemical Aging Conditions in a Smog Chamber, Environ Sci Technol, 52, 4979-4988, 10.1021/acs.est.7b06269, 2018.

Henry, K. M., and Donahue, N. M.: Photochemical Aging of alpha-Pinene Secondary Organic Aerosol: Effects of OH Radical Sources and Photolysis, J Phys Chem A, 116, 5932-5940, 10.1021/jp210288s, 2012.

Hettiyadura, A. P. S., Stone, E. A., Kundu, S., Baker, Z., Geddes, E., Richards, K., and Humphry, T.: Determination of atmospheric organosulfates using HILIC chromatography with MS detection, Atmos Meas Tech, 8, 2347-2358, 10.5194/amt-8-2347-2015, 2015.

Hodzic, A., Kasibhatla, P. S., Jo, D. S., Cappa, C. D., Jimenez, J. L., Madronich, S., and Park, R. J.: Rethinking the global secondary organic aerosol (SOA) budget: stronger production, faster removal, shorter lifetime, Atmospheric Chemistry and Physics, 16, 7917-7941, 10.5194/acp-16-7917-2016, 2016.

Huang, J. P., Mcqueen, J., Wilczak, J., Djalalova, I., Stajner, I., Shafran, P., Allured, D., Lee, P., Pan, L., Tong, D., Huang, H. C., Dimego, G., Upadhayay, S., and Monache, L. D.: Improving NOAA NAQFC PM2.5 Predictions with a Bias Correction Approach, Weather Forecast, 32, 407-421, 10.1175/Waf-D-16-0118.1, 2017.

Huang, M. Q., Zhang, J. H., Cai, S. Y., Liao, Y. M., Zhao, W. X., Hu, C. J., Gu, X. J., Fang, L., and Zhang, W. J.: Characterization of particulate products for aging of ethylbenzene secondary organic aerosol in the presence of ammonium sulfate seed aerosol, J Environ Sci-China, 47, 219-229, 10.1016/j.jes.2015.11.033, 2016.

Im, Y., Jang, M., and Beardsley, R. L.: Simulation of aromatic SOA formation using the lumping model integrated with explicit gas-phase kinetic mechanisms and aerosol-phase reactions, Atmospheric Chemistry and Physics, 14, 4013-4027, 10.5194/acp-14-4013-2014, 2014.

IPCC: Climate change 2014: mitigation of climate change, Cambridge University Press, 2015.

Jang, M., and Kamens, R. M.: A thermodynamic approach for modeling partitioning of semivolatile organic compounds on atmospheric particulate matter: Humidity effects, Environmental Science & Technology, 32, 1237-1243, Doi 10.1021/Es970773w, 1998.

Jang, M., Czoschke, N. M., Lee, S., and Kamens, R. M.: Heterogeneous atmospheric aerosol production by acid-catalyzed particle-phase reactions, Science, 298, 814-817, 10.1126/science.1075798, 2002.

Jang, M. S., and Kamens, R. M.: Characterization of secondary aerosol from the photooxidation of toluene in the presence of NOx and 1-propene, Environmental Science & Technology, 35, 3626-3639, 10.1021/es010676+, 2001.

Jang, M. S., Czoschke, N. M., and Northcross, A. L.: Semiempirical model for organic aerosol growth by acid-catalyzed heterogeneous reactions of organic carbonyls, Environmental Science & Technology, 39, 164-174, 10.1021/es048977h, 2005.

Jathar, S. H., Cappa, C. D., Wexler, A. S., Seinfeld, J. H., and Kleeman, M. J.: Simulating secondary organic aerosol in a regional air quality model using the statistical oxidation model - Part 1: Assessing the influence of constrained multi-generational ageing, Atmospheric Chemistry and Physics, 16, 2309-2322, 10.5194/acp-16-2309-2016, 2016.

Jeffries, H., Gary, M., Kessler, M., and Sexton, K.: Morphecule reaction mechanism, MORPHO, ALLOMORPHIC simulation software, Technical Report CR813107, CR813964 and CR815779, 1998.

Jenkin, M. E., Wyche, K. P., Evans, C. J., Carr, T., Monks, P. S., Alfarra, M. R., Barley, M. H., McFiggans, G. B., Young, J. C., and Rickard, A. R.: Development and chamber evaluation of the MCM v3.2 degradation scheme for beta-caryophyllene, Atmospheric Chemistry and Physics, 12, 5275-5308, 10.5194/acp-12-5275-2012, 2012.

Jiang, H., Jang, M., and Yu, Z. C.: Dithiothreitol activity by particulate oxidizers of SOA produced from photooxidation of hydrocarbons under varied NOx levels, Atmospheric Chemistry and Physics, 17, 9965-9977, 10.5194/acp-17-9965-2017, 2017.

Jimenez, J. L., Canagaratna, M. R., Donahue, N. M., Prevot, A. S. H., Zhang, Q., Kroll, J. H., DeCarlo, P. F., Allan, J. D., Coe, H., Ng, N. L., Aiken, A. C., Docherty, K. S., Ulbrich, I. M., Grieshop, A. P., Robinson, A. L., Duplissy, J., Smith, J. D., Wilson, K. R., Lanz, V. A., Hueglin, C., Sun, Y. L., Tian, J., Laaksonen, A., Raatikainen, T., Rautiainen, J., Vaattovaara, P., Ehn, M., Kulmala, M., Tomlinson, J. M., Collins, D. R., Cubison, M. J., Dunlea, E. J., Huffman, J. A., Onasch, T. B., Alfarra, M. R., Williams, P. I., Bower, K., Kondo, Y., Schneider, J., Drewnick, F., Borrmann, S., Weimer, S., Demerjian, K., Salcedo, D., Cottrell, L., Griffin, R., Takami, A., Miyoshi, T., Hatakeyama, S., Shimono, A., Sun, J. Y., Zhang, Y. M., Dzepina, K., Kimmel, J. R., Sueper, D., Jayne, J. T., Herndon, S. C., Trimborn, A. M., Williams, L. R., Wood, E. C., Middlebrook, A. M., Kolb, C. E., Baltensperger, U., and Worsnop, D. R.: Evolution of Organic Aerosols in the Atmosphere, Science, 326, 1525-1529, 10.1126/science.1180353, 2009.

Johnson, D., Jenkin, M. E., Wirtz, K., and Martin-Reviejo, M.: Simulating the Formation of Secondary Organic Aerosol from the Photooxidation of Toluene, Environmental Chemistry, 1, 150-165, 10.1071/EN04069, 2004.

Johnson, D., Jenkin, M. E., Wirtz, K., and Martin-Reviejo, M.: Simulating the formation of secondary organic aerosol from the photooxidation of aromatic hydrocarbons, Environmental Chemistry, 2, 35-48, 10.1071/EN04079, 2005.

Kamens, R. M., Zhang, H. F., Chen, E. H., Zhou, Y., Parikh, H. M., Wilson, R. L., Galloway, K. E., and Rosen, E. P.: Secondary organic aerosol formation from toluene in an atmospheric hydrocarbon mixture: Water and particle seed effects, Atmospheric Environment, 45, 2324-2334, 10.1016/j.atmosenv.2010.11.007, 2011.

Kelly, J. M., Doherty, R. M., O'Connor, F. M., and Mann, G. W.: The impact of biogenic, anthropogenic, and biomass burning volatile organic compound emissions on regional and seasonal variations in secondary organic aerosol, Atmospheric Chemistry and Physics, 18, 7393-7422, 10.5194/acp-18-7393-2018, 2018.

Kleindienst, T. E., Edney, E. O., Lewandowski, M., Offenberg, J. H., and Jaoui, M.: Secondary organic carbon and aerosol yields from the irradiations of isoprene and alpha-pinene in the presence of NOx and SO2, Environmental Science & Technology, 40, 3807-3812, 10.1021/es052446r, 2006.

Kleindienst, T. E., Jaoui, M., Lewandowski, M., Offenberg, J. H., Lewis, C. W., Bhave, P. V., and Edney, E. O.: Estimates of the contributions of biogenic and anthropogenic hydrocarbons to secondary organic aerosol at a southeastern US location, Atmospheric Environment, 41, 8288-8300, 10.1016/j.atmosenv.2007.06.045, 2007.

Kolska, Z., Ruzicka, V., and Gani, R.: Estimation of the enthalpy of vaporization and the entropy of vaporization for pure organic compounds at 298.15 K and at normal boiling temperature by a group contribution method, Industrial & Engineering Chemistry Research, 44, 8436-8454, 10.1021/ie050113x, 2005.

Lambe, A. T., Onasch, T. B., Croasdale, D. R., Wright, J. P., Martin, A. T., Franklin, J. P., Massoli, P., Kroll, J. H., Canagaratna, M. R., Brune, W. H., Worsnop, D. R., and Davidovits, P.: Transitions from Functionalization to Fragmentation Reactions of Laboratory Secondary Organic Aerosol (SOA) Generated from the OH Oxidation of Alkane Precursors, Environmental Science & Technology, 46, 5430-5437, 10.1021/es300274t, 2012.

Li, J., Jang, M., and Beardsley, R. L.: Dialkylsulfate formation in sulfuric acid-seeded secondary organic aerosol produced using an outdoor chamber under natural sunlight, Environmental Chemistry, 13, 590-601, 2016a.

Li, J. Y., and Jang, M.: Aerosol Acidity Measurement Using Colorimetry Coupled With a Reflectance UV-Visible Spectrometer, Aerosol Science and Technology, 46, 833-842, 10.1080/02786826.2012.669873, 2012.

Li, L., Tang, P., and Cocker, D. R.: Instantaneous nitric oxide effect on secondary organic aerosol formation from m-xylene photooxidation, Atmospheric Environment, 119, 144-155, 2015.

Li, L. J., Tang, P., Nakao, S., and Cocker, D. R.: Impact of molecular structure on secondary organic aerosol formation from aromatic hydrocarbon photooxidation under low-NOx conditions, Atmospheric Chemistry and Physics, 16, 10793-10808, 10.5194/acp-16-10793-2016, 2016b.

Li, M., Zhang, Q., Kurokawa, J., Woo, J. H., He, K. B., Lu, Z. F., Ohara, T., Song, Y., Streets, D. G., Carmichael, G. R., Cheng, Y. F., Hong, C. P., Huo, H., Jiang, X. J., Kang, S. C., Liu, F., Su, H., and Zheng, B.: MIX: a mosaic Asian anthropogenic emission inventory under the international collaboration framework of the MICS-Asia and HTAP, Atmospheric Chemistry and Physics, 17, 935-963, 10.5194/acp-17-935-2017, 2017.

Lin, Y. H., Knipping, E. M., Edgerton, E. S., Shaw, S. L., and Surratt, J. D.: Investigating the influences of SO2 and NH3 levels on isoprene-derived secondary organic aerosol formation using conditional sampling approaches, Atmospheric Chemistry and Physics, 13, 8457-8470, 10.5194/acp-13-8457-2013, 2013.

Liu, T. Y., Huang, D. D., Li, Z. J., Liu, Q. Y., Chan, M. N., and Chan, C. K.: Comparison of secondary organic aerosol formation from toluene on initially wet and dry ammonium sulfate particles at moderate relative humidity, Atmospheric Chemistry and Physics, 18, 5677-5689, 10.5194/acp-18-5677-2018, 2018.

McDonald, B. C., de Gouw, J. A., Gilman, J. B., Jathar, S. H., Akherati, A., Cappa, C. D., Jimenez, J. L., Lee-Taylor, J., Hayes, P. L., McKeen, S. A., Cui, Y. Y., Kim, S. W., Gentner, D. R., Isaacman-VanWertz, G., Goldstein, A. H., Harley, R. A., Frost, G. J., Roberts, J. M., Ryerson, T. B., and Trainer, M.: Volatile chemical products emerging as largest petrochemical source of urban organic emissions, Science, 359, 760-764, ARTN aaq0524
10.1126/science.aaq0524, 2018.

McNeill, V. F., Woo, J. L., Kim, D. D., Schwier, A. N., Wannell, N. J., Sumner, A. J., and Barakat, J. M.: Aqueous-Phase Secondary Organic Aerosol and Organosulfate Formation in Atmospheric Aerosols: A Modeling Study, Environmental Science & Technology, 46, 8075-8081, 10.1021/es3002986, 2012.

Mcvay, R. C., Cappa, C. D., and Seinfeld, J. H.: Vapor-Wall Deposition in Chambers: Theoretical Considerations, Environmental Science & Technology, 48, 10251-10258, 10.1021/es502170j, 2014.

Molteni, U., Bianchi, F., Klein, F., El Haddad, I., Frege, C., Rossi, M. J., Dommen, J., and Baltensperger, U.: Formation of highly oxygenated organic molecules from aromatic compounds, Atmospheric Chemistry and Physics, 18, 1909-1921, 10.5194/acp-18-1909-2018, 2018.

Nakao, S., Clark, C., Tang, P., Sato, K., and Cocker, D.: Secondary organic aerosol formation from phenolic compounds in the absence of NOx, Atmospheric Chemistry and Physics, 11, 10649-10660, 10.5194/acp-11-10649-2011, 2011.

Ng, N. L., Kroll, J. H., Chan, A. W. H., Chhabra, P. S., Flagan, R. C., and Seinfeld, J. H.: Secondary organic aerosol formation from m-xylene, toluene, and benzene, Atmospheric Chemistry and Physics, 7, 3909-3922, DOI 10.5194/acp-7-3909-2007, 2007.

Noziere, B., Ekstrom, S., Alsberg, T., and Holmstrom, S.: Radical-initiated formation of organosulfates and surfactants in atmospheric aerosols, Geophys Res Lett, 37, Artn L05806
10.1029/2009gl041683, 2010.

Odian, G.: Principles of polymerization, John Wiley & Sons, 2004.

Odum, J. R., Hoffmann, T., Bowman, F., Collins, D., Flagan, R. C., and Seinfeld, J. H.: Gas/particle partitioning and secondary organic aerosol yields, Environmental Science & Technology, 30, 2580-2585, Doi 10.1021/Es950943+, 1996.

Pankow, J. F.: An Absorption-Model of Gas-Particle Partitioning of Organic-Compounds in the Atmosphere, Atmospheric Environment, 28, 185-188, Doi 10.1016/1352-2310(94)90093-0, 1994.

Press, W. H., Teukolsky, S. A., Vetterling, W. T., and Flannery, B. P.: Numerical recipes in Fortran 77: the art of scientific computing, Cambridge university press Cambridge, 1992.

Ren, J. Y., Zhang, F., Wang, Y. Y., Collins, D., Fan, X. X., Jin, X. A., Xu, W. Q., Sun, Y. L., Cribb, M., and Li, Z. Q.: Using different assumptions of aerosol mixing state and chemical composition to predict CCN concentrations based on field measurements in urban Beijing, Atmospheric Chemistry and Physics, 18, 6907-6921, 10.5194/acp-18-6907-2018, 2018.

Requia, W. J., Higgins, C. D., Adams, M. D., Mohamed, M., and Koutrakis, P.: The health impacts of weekday traffic: A health risk assessment of PM2.5 emissions during congested periods, Environ Int, 111, 164-176, 10.1016/j.envint.2017.11.025, 2018.

Rudich, Y., Donahue, N. M., and Mentel, T. F.: Aging of organic aerosol: Bridging the gap between laboratory and field studies, Annu. Rev. Phys. Chem., 58, 321-352, 2007.

Sato, K., Hatakeyama, S., and Imamura, T.: Secondary organic aerosol formation during the photooxidation of toluene: NOx dependence of chemical composition, J Phys Chem A, 111, 9796-9808, 10.1021/jp071419f, 2007.

Sato, K., Takami, A., Kato, Y., Seta, T., Fujitani, Y., Hikida, T., Shimono, A., and Imamura, T.: AMS and LC/MS analyses of SOA from the photooxidation of benzene and 1,3,5-trimethylbenzene in the presence of NOx: effects of chemical structure on SOA aging, Atmospheric Chemistry and Physics, 12, 4667-4682, 10.5194/acp-12-4667-2012, 2012.

Schell, B., Ackermann, I. J., Hass, H., Binkowski, F. S., and Ebel, A.: Modeling the formation of secondary organic aerosol within a comprehensive air quality model system, J Geophys Res-Atmos, 106, 28275-28293, Doi 10.1029/2001jd000384, 2001.

Seinfeld, J. H., and Pandis, S. N.: Atmospheric chemistry and physics: from air pollution to climate change, John Wiley & Sons, 2016.

Sheehan, P. E., and Bowman, F. M.: Estimated effects of temperature on secondary organic aerosol concentrations, Environ Sci Technol, 35, 2129-2135, Doi 10.1021/Es001547g, 2001.

Shilling, J. E., King, S. M., Mochida, M., and Martin, S. T.: Mass spectral evidence that small changes in composition caused by oxidative aging processes alter aerosol CCN properties, J Phys Chem A, 111, 3358-3368, 10.1021/jp068822r, 2007.

Song, C., Na, K. S., and Cocker, D. R.: Impact of the hydrocarbon to NOx ratio on secondary organic aerosol formation, Environmental Science & Technology, 39, 3143-3149, 10.1021/es0493244, 2005.

Surratt, J. D., Chan, A. W. H., Eddingsaas, N. C., Chan, M. N., Loza, C. L., Kwan, A. J., Hersey, S. P., Flagan, R. C., Wennberg, P. O., and Seinfeld, J. H.: Reactive intermediates revealed in secondary organic aerosol formation from isoprene, P Natl Acad Sci USA, 107, 6640-6645, 10.1073/pnas.0911114107, 2010.

Tsigaridis, K., Daskalakis, N., Kanakidou, M., Adams, P. J., Artaxo, P., Bahadur, R., Balkanski, Y., Bauer, S. E., Bellouin, N., Benedetti, A., Bergman, T., Berntsen, T. K., Beukes, J. P., Bian, H., Carslaw, K. S., Chin, M., Curci, G., Diehl, T., Easter, R. C., Ghan, S. J., Gong, S. L., Hodzic, A., Hoyle, C. R., Iversen, T., Jathar, S., Jimenez, J. L., Kaiser, J. W., Kirkevag, A., Koch, D., Kokkola, H., Lee, Y. H., Lin, G., Liu, X., Luo, G., Ma, X., Mann, G. W., Mihalopoulos, N., Morcrette, J. J., Muller, J. F., Myhre, G., Myriokefalitakis, S., Ng, N. L., O'Donnell, D., Penner, J. E., Pozzoli, L., Pringle, K. J., Russell, L. M., Schulz, M., Sciare, J., Seland, O., Shindell, D. T., Sillman, S., Skeie, R. B., Spracklen, D., Stavrakou, T., Steenrod, S. D., Takemura, T., Tiitta, P., Tilmes, S., Tost, H., van Noije, T., van Zyl, P. G., von Salzen, K., Yu, F., Wang, Z., Wang, Z., Zaveri, R. A., Zhang, H., Zhang, K., Zhang, Q., and Zhang, X.: The AeroCom evaluation and intercomparison of organic aerosol in global models, Atmospheric Chemistry and Physics, 14, 10845-10895, 10.5194/acp-14-10845-2014, 2014.

Wood, E. C., Canagaratna, M. R., Herndon, S. C., Onasch, T. B., Kolb, C. E., Worsnop, D. R., Kroll, J. H., Knighton, W. B., Seila, R., Zavala, M., Molina, L. T., DeCarlo, P. F., Jimenez, J. L., Weinheimer, A. J., Knapp, D. J., Jobson, B. T., Stutz, J., Kuster, W. C., and Williams, E. J.: Investigation of the correlation between odd oxygen and secondary organic aerosol in Mexico City and Houston, Atmospheric Chemistry and Physics, 10, 8947-8968, 10.5194/acp-10-8947-2010, 2010.

Yu, Z. C., Jang, M., and Park, J.: Modeling atmospheric mineral aerosol chemistry to predict heterogeneous photooxidation of SO2, Atmospheric Chemistry and Physics, 17, 10001-10017, 10.5194/acp-17-10001-2017, 2017.

Zhang, X., Cappa, C. D., Jathar, S. H., Mcvay, R. C., Ensberg, J. J., Kleeman, M. J., and Seinfeld, J. H.: Influence of vapor wall loss in laboratory chambers on yields of secondary organic aerosol, P Natl Acad Sci USA, 111, 5802-5807, 10.1073/pnas.1404727111, 2014.

Zhang, Y., Seigneur, C., Seinfeld, J. H., Jacobson, M., Clegg, S. L., and Binkowski, F. S.: A comparative review of inorganic aerosol thermodynamic equilibrium modules: similarities, differences, and their likely causes, Atmospheric Environment, 34, 117-137, Doi 10.1016/S1352-2310(99)00236-8, 2000.

Zhang, Y. L., Yang, W. Q., Simpson, I., Huang, X. Y., Yu, J. Z., Huang, Z. H., Wang, Z. Y., Zhang, Z., Liu, D., Huang, Z. Z., Wang, Y. J., Pei, C. L., Shao, M., Blake, D. R., Zheng, J. Y., Huang, Z. J., and Wang, X. M.: Decadal changes in emissions of volatile organic compounds (VOCs) from on-road vehicles with intensified automobile pollution control: Case study in a busy urban tunnel in south China, Environ Pollut, 233, 806-819, 10.1016/j.envpol.2017.10.133, 2018.

Zhao, B., Wang, S. X., Donahue, N. M., Chuang, W. N., Hildebrandt Ruiz, L., Ng, N. L., Wang, Y. J., and Hao, J. M.: Evaluation of One-Dimensional and Two-Dimensional Volatility Basis Sets in Simulating the Aging of Secondary Organic Aerosol with Smog-Chamber Experiments, Environmental Science & Technology, 49, 2245-2254, 10.1021/es5048914, 2015.

Zhao, L. W., Li, P., and Yalkowsky, S. H.: Predicting the entropy of boiling for organic compounds, J Chem Inf Comp Sci, 39, 1112-1116, Doi 10.1021/Ci990054w, 1999.

Zuend, A., Marcolli, C., Booth, A. M., Lienhard, D. M., Soonsin, V., Krieger, U. K., Topping, D. O., McFiggans, G., Peter, T., and Seinfeld, J. H.: New and extended parameterization of the thermodynamic model AIOMFAC: calculation of activity coefficients for organic-inorganic mixtures containing carboxyl, hydroxyl, carbonyl, ether, ester, alkenyl, alkyl, and aromatic functional groups, Atmospheric Chemistry and Physics, 11, 9155-9206, 10.5194/acp-11-9155-2011, 2011.

Table 1: Experimental conditions and resulting SOA chamber data of the monoalkylbenzenes photooxidation experiments performed under various NO_x conditions with or without inorganic seeded aerosol in the dual outdoor UF APHOR chambers.

		Initial condition							
Exp. ID [a]	Date [b]	HC (ppb)	NO_x (HONO) (ppb)	Seeded aerosol [d] ($\mu g/m^3$)	HC/NO_x (ppbC/ppb)	Y_{SOA} [e] (%)	RH (%)	Temperature (K)	Note [f]
Tol1	01/06/12 E [c]	190	110 (40)	50	12.1	18.9	18-81	280–306	Fig. 6(a)
Tol2	01/06/12 W [c]	190	95 (35)	-	14.8	13.3	18-81	280–306	Fig. 6(a)
Tol3	02/09/12 E [c]	175	245 (35)	46	5.0	15.3	21-83	280–307	Fig. 6(d)
Tol4	02/09/12 W [c]	180	246 (35)	-	4.5	9.3	21-84	280–307	Fig. 6(d)
Tol5	06/20/12 E [c]	165	110 (15)	35 (SA)	10.5	15.6	27-83	295–317	Fig. S7(a)
Tol6	12/16/17 E	198	132 (79)	-	10.5	8.6	23-58	283-300	Fig. 3(a) and Fig. S7(b)
Tol7	02/25/18 W	154	170 (22)	-	6.4	3.3	20-44	293-313	Fig. 3(b), Fig. S3(a) and Fig. S7(c)
Tol8	04/30/18 E	127	306 (47)	70 (SA)	2.9	13.1	14-57	289-317	Fig. 3(c), Fig. 5(a) and Fig. S7(d)
Tol9	06/14/18 W	135	361 (80)	130 (wAS)	2.6	19.0	51-98	295-319	Fig. S7(e)
EB1	12/05/17 E	126	71 (32)	43	14.2	15.4	18-57	287-310	Fig. 6(b)
EB2	12/05/17 W	134	74 (38)	-	14.4	12.2	25-66	288-310	Fig. 6(b) and Fig. S3(b)
EB3	01/04/18 E	132	175 (13)	50	6.0	21.8	30-85	267-291	Fig. S7(f)
EB4	01/04/18 W	131	175 (22)	-	6.0	12.8	48-93	267-289	Fig. S7(f)
EB5	12/10/17 E	131	363 (13)	39	2.9	10.1	20-83	271-298	Fig. 6(e)
EB6	12/10/17 W	128	363 (15)	-	2.8	4.1	33-86	272-295	Fig. 6(e)
EB7	02/19/18 W	125	81 (36)	80 (SA)	12.3	25.6	19-46	292-315	Fig. 5(b) and Fig. S7(g)
EB8	02/19/18 E	112	63 (36)	35 (dAS)	14.3	11.0	13-39	292-314	Fig. S7(g)
EB9	01/19/18 W	169	106 (30)	40 (wAS)	12.7	28.6	20-87	269-302	Fig. S7(h)
PB1	03/04/18 E	100	87 (19)	57	10.4	7.4	11-54	279-306	Fig. 6(c)
PB2	03/04/18 W	109	108 (24)	-	9.1	5.4	17-59	279-305	Fig. 6(c) and Fig. S3(c)
PB3	03/28/18 E	87	264 (36)	54	3.0	7.1	11-43	285-312	Fig. 6(f)
PB4	03/28/18 W	88	248 (33)	-	3.2	4.6	16-51	285-312	Fig. 6(f)
PB5	04/05/18 W	101	76 (35)	70 (SA)	12.0	15.7	30-93	282-312	Fig. 5(c) and Fig. S7(i)
PB6	04/17/18 E	101	149 (141)	70 (SA)	6.1	11.9	14-85	278-313	Fig. S7(j)
PB7	04/17/18 W	101	155 (126)	70 (wAS)	5.9	18.1	40-91	279-310	Fig. S7(j)
PB8	06/14/18 E	83	353 (148)	90 (SA)	2.1	10.7	22-90	294-322	Fig. S7(k)

[a] “Tol”, “EB”, and “PB” represent toluene, ethylbenzene, and n-propylbenzene oxidation experiments, respectively.

[b] “E” or “W” denotes the east or west chamber.

[c] SOA data obtained from Im et al. (2014).

[d] “SA”, “wAS”, and “dAS” denote sulfuric acid seeds, wet ammonium sulfate seeds, and dry ammonium sulfate seeds. (dry: RH < ERH; wet: RH > ERH). For those without notification, SO_2 (in the unit of ppb) was injected into the chamber to generate acidic seeds.

[e] SOA yield is estimated using $Y_{SOA} = \Delta OM/\Delta HC$, where ΔOM is formed organic matter, ΔHC is consumed HC. Yield in the table was estimated where SOA mass reached to the maximum over the course of the experiments.

[f] This column denotes that the corresponding data was used in which figures.

The accuracy of RH is 5 %. The accuracy of temperature is 0.5 K.

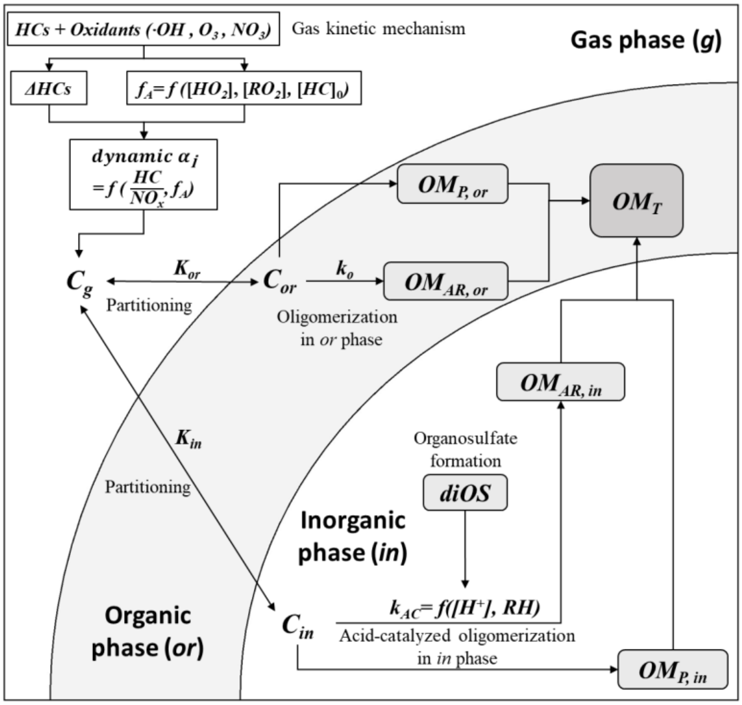

Figure 1: Simplified scheme of the UNIPAR model. [*HC*]$_0$ represent the initial hydrocarbon (HC) concentration. The dynamic mass-based stoichiometric coefficient (dynamic α_i), the consumption of HCs (ΔHCs), and the concentrations of hydroperoxide radical ([HO_2]) and organic peroxyl radical ([RO_2]) are simulated from the gas kinetic model. The aging factor (f_A) is represented as a function of [HO_2], [RO_2], and [*HC*]$_0$, which is detailed in Section 3.1. *C* and *K* denote the concentration and the partitioning coefficient in gas phase (*g*), organic phase (*or*), and inorganic phase (*in*). $k_{or,i}$ denotes the reaction rate constant of oligomerization in *or* phase. $k_{AC,i}$ denotes the reaction rate constant of acid-catalyzed oligomerization in *in* phase and is represented as a function of aerosol acidity ([H^+]) and ambient humidity (RH). *OM* represents the concentration of organic matter. Subscripts, "*AR*", "*P*", and "*T*" denote aerosol-phase reactions, partitioning, and total organic matter, respectively. Subscript *i* represents each lumping species. *diOS* represents the concentration of organosulfate (dialkyl sulfate (diOS) in this study).

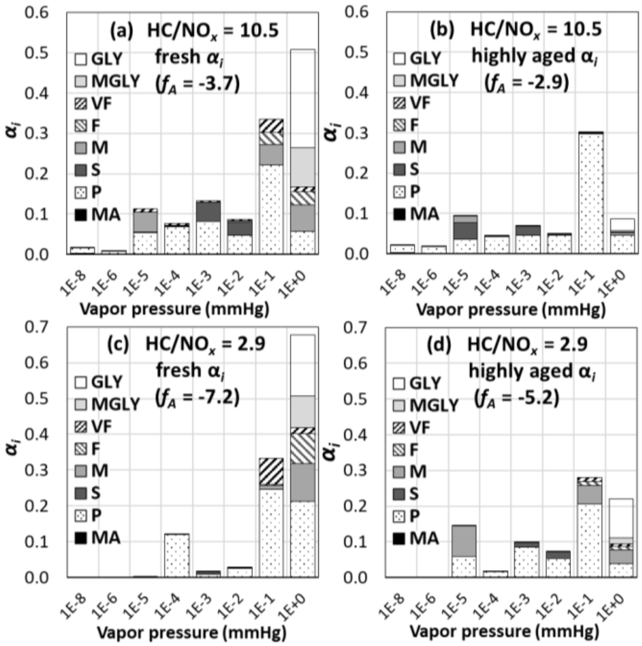

Figure 2: The mass-based stoichiometric coefficients (α_i) of each species, *i*, from toluene oxidation under low NO$_x$ level (simulation based on the sunlight of Exp. Tol6, HC/NO$_x$ = 10.5, 12/16/18) at (a) fresh condition and (b) highly aged condition, and under high NO$_x$ level (simulation based on the sunlight of Exp. Tol8, HC/NO$_x$ = 2.9, 04/30/18) at (c) fresh condition and (d) highly aged condition, where f_A is the aging factor as derived in Eq. 1. The oxygenated products predicted by the explicit gas kinetic model are lumped as a function of vapor pressure (8 groups: 10^{-8}, 10^{-6}, 10^{-5}, 10^{-4}, 10^{-3}, 10^{-2}, 10^{-1}, and 1 mmHg) and aerosol phase reactivity (6 groups), i.e., very fast (VF: tricarbonyls and *α*-hydroxybicarbonyls), fast (F: 2 epoxides or aldehydes,), medium (M: 1 epoxide or aldehyde), slow (S: ketones), partitioning only (P), and multialcohol (MA). MGLY (methylglyoxal) and GLY (glyoxal) were lumped separately due to the relatively high reactivity.

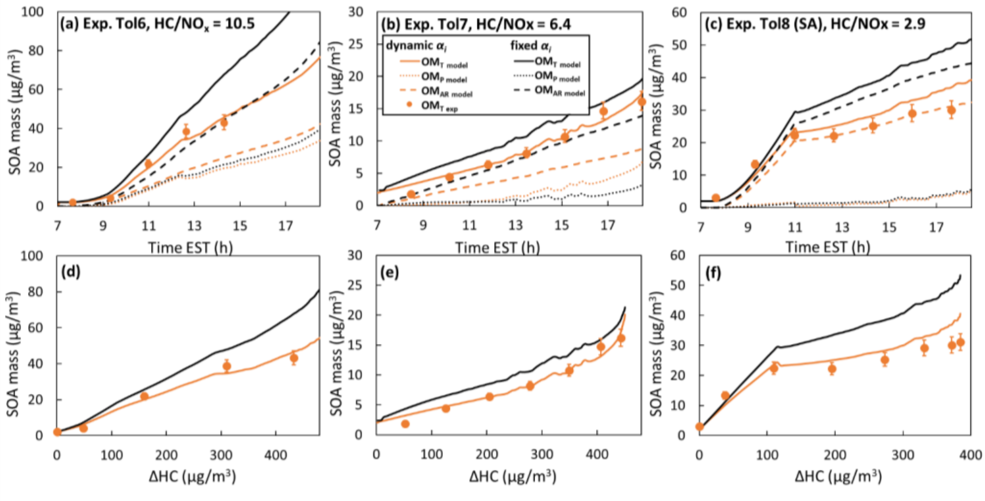

Figure 3: Comparison between simulated SOA mass by the fixed α_i (α fixed at the point of HC being consumed half of the total consumption) and dynamic α_i (α evolving as photooxidation) under (a) low NO$_x$ condition (Exp. Tol6, HC/NO$_x$ = 10.5), (b) moderate NO$_x$ condition (Exp. Tol7, HC/NO$_x$ = 6.4), and (c) high NO$_x$ condition (Exp. Tol8, HC/NO$_x$ = 2.9 with sulfuric acid (SA) seeded aerosol). (d), (e), and (f) represent the time-dependent SOA growth curve (SOA mass concentration against consumed HC) corresponding to the experimental conditions of (a), (b), and (c), respectively. The solid circle represents the experimental measurements. The SOA mass is corrected for particle loss to the chamber wall. The experimental conditions are available in Table 1.

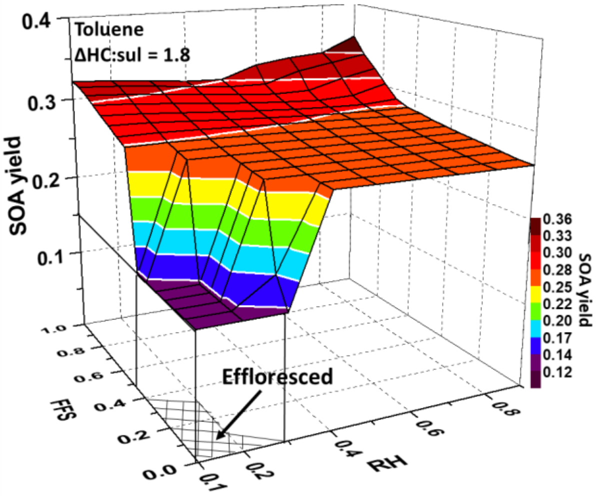

Figure 4: Simulated toluene SOA yields ($Y_{SOA} = \Delta OM/\Delta HC$) as a function of relative humidity (RH: 0.1 ~ 0.9) and fractional free sulfate (FFS: 0 ~ 1), where FFS = ($[SO_4^{2-}]-0.5[NH_4^+])/[SO_4^{2-}]$) and is used to estimate aerosol acidity ($[H^+]$) in inorganic thermodynamic model. The RH and FFS are fixed in the simulations. The gas-phase simulations are based on the experimental condition of 06/14/2018 (Exp. Tol9 in Table 1) (initial HC concentration = 20 ppb, HC/NO_x = 2, sulfate mass concentration = 20 μg/m^3, and the mass ratio of the consumed HC to sulfate (ΔHC:sulf) = 1.5).

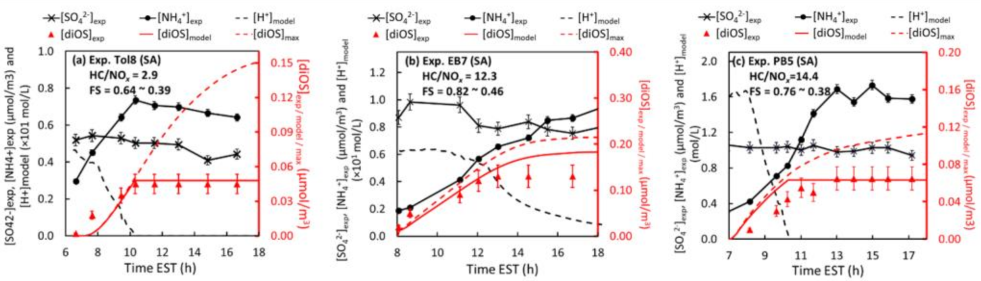

Figure 5: Time profiles of measured inorganic sulfate concentration ($[SO_4^{2-}]_{exp}$), ammonium concentration ($[NH_4^+]_{exp}$), diOS concentration ($[diOS]_{exp}$), the predicted proton concentration ($[H^+]$), diOS concentration ($[diOS]_{model}$), and the maximum diOS concentration ($[diOS]_{max}$) (assuming there is no ammonia neutralization in the system) for SOA generated from (a) toluene (HC/NO_x = 2.9, OM-to-sulfate mass ratio (OM:sulf) = 1.4), (b) ethylbenzene (HC/NO_x = 12.3, OM:sulf = 1.4), and (c) n-propylbenzene (HC/NO_x = 14.4, OM:sulf = 0.7). The degree of neutralization is indicated by FS, which is ranging from 1 (for sulfuric acid) to 0.33 (for ammonium sulfate). "SA" stands for experiment with direct-injection sulfuric acid seeded aerosols. The ion and diOS concentrations were corrected for the particle loss to the chamber wall. The experimental conditions are available in Table 1.

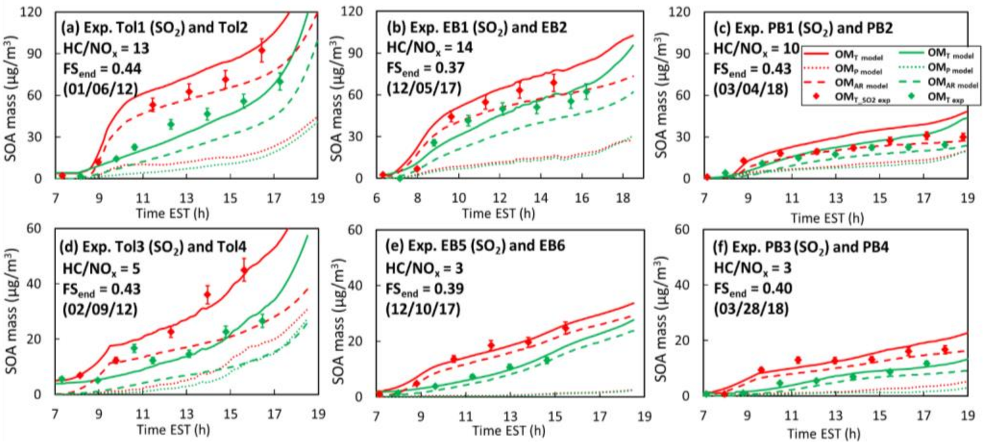

Figure 6: Time profiles of measured and modeled SOA mass concentrations for toluene, ethylbenzene, and n-propylbenzene SOA under low/high NO$_x$ conditions in the presence/absence of SO$_2$-derived sulfuric acid seeded aerosol. The red and green colors indicate experiments with and without SO$_2$, respectively. Solid, dashed, and dotted lines denote the total organic matter (OM$_T$), the OM from partitioning only (OM$_P$), and the OM from the aerosol-phase reactions (OM$_{AR}$), respectively. The degree of ammonia neutralization with sulfuric acid is indicated by the FS$_{end}$, which is the FS at the end of the experimental run. The FS$_{end}$ is ranging from 1 (for sulfuric acid) to 0.33 (for ammonium sulfate). The uncertainty associated with experimentally measured OM is about 9 %. The SOA mass was corrected for the particle loss to the wall. The experimental conditions are available in Table 1.

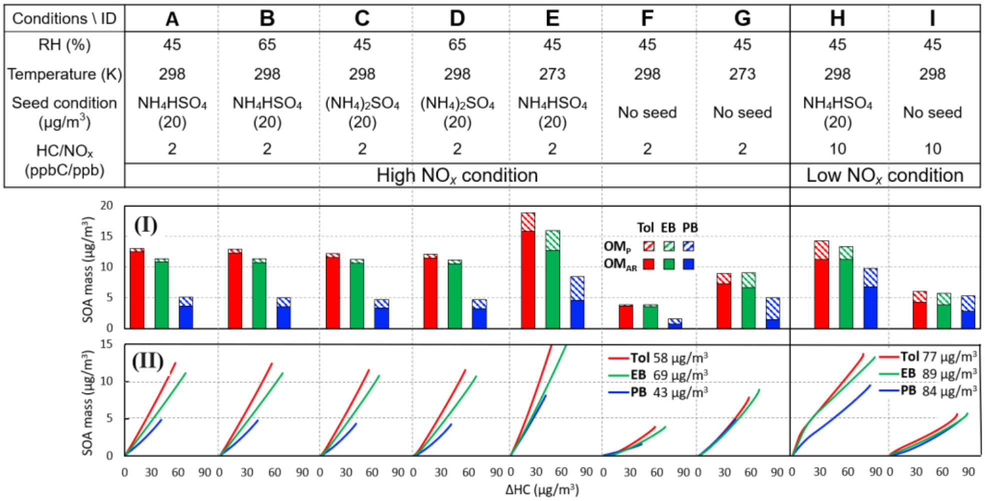

Conditions \ ID	A	B	C	D	E	F	G	H	I
RH (%)	45	65	45	65	45	45	45	45	45
Temperature (K)	298	298	298	298	273	298	273	298	298
Seed condition ($\mu g/m^3$)	NH_4HSO_4 (20)	NH_4HSO_4 (20)	$(NH_4)_2SO_4$ (20)	$(NH_4)_2SO_4$ (20)	NH_4HSO_4 (20)	No seed	No seed	NH_4HSO_4 (20)	No seed
HC/NO_x (ppbC/ppb)	2	2	2	2	2	2	2	10	10
	High NO_x condition							Low NO_x condition	

Figure 7: The simulated SOA mass (Panel I) for toluene (Tol), ethylbenzene (EB) and n-propylbenzene (PB) under different conditions, as are listed the top table. The initial concentrations of monoalkylbenzenes, pre-existing OM (OM_0), NH_4HSO_4 (AHS) seeded aerosol, and $(NH_4)_2SO_4$ (AS) seeded aerosol are set at 20 ppb, 2 µg/m^3, 20 µg/m^3, and 20 µg/m^3, respectively. The gas-phase simulation used the sunlight on 06/14/2018 (Exp. Tol9 in Table 1). OM_P and OM_{AR} represent the organic matter from the partitioning process and aerosol-phase reactions. (Panel II) shows the time-dependent SOA growth curve for three monoalkylbenzenes under corresponding conditions (top table). The concentrations in the legends refer to the mass concentrations of the consumed hydrocarbons in each simulation under the high/low NO_x conditions.